



Numerical simulations of cavitating flow

Master thesis

Study programme: N2301 – Mechanical Engineering
Study branch: 2302T010 – Machines and Equipment Design
Author: **Hiren Narendrakumar Rashiwala**
Supervisor: Ing. Miloš Müller, Ph.D.



DIPLOMA THESIS ASSIGNMENT

(PROJECT, ART WORK, ART PERFORMANCE)

First name and surname: **Hiren Narendrakumar Rashiwala**
Study program: **N2301 Mechanical Engineering**
Identification number: **S15000605**
Specialization: **Machines and Equipment Design**
Topic name: **Numerical simulations of cavitating flow**
Assigning department: **Department of Power Engineering Equipment**

R u l e s f o r e l a b o r a t i o n :

1. Current approaches used for simulations of cavitating flow.
2. Physical models used for the description of the cavitation erosion potential.
3. Creation of a simulation model (CFD) according to the real experiment in the cavitation tunnel.
4. Testing of numerical models for cavitating flow simulations in selected regimes.
5. Comparison of the simulations with the experiments in the cavitation tunnel.
6. Prediction of the cavitation damage for the tested geometry.

Scope of graphic works: 10
Scope of work report
(scope of dissertation): 40 stran
Form of dissertation elaboration: printed
List of specialized literature:

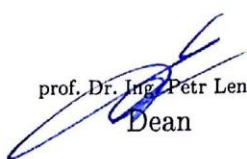
[1] KINZEL, M. P., *Computational Techniques and Analysis of Cavitating-Fluid Flows, Dissertation. 2008.*

[2] Luca D'Agostino; Maria Vittoria Salvetti, *Fluid Dynamics of Cavitation and Cavitating Turbopumps. Springer, cop. 2007.*

[3] BRENNEN, Christopher Earls, *Cavitation and Bubble Dynamics. Oxford University Press , New York, 1995.*

[4] FRANC, J., MICHEL, J. M., *Fundamentals of cavitation. In Fluid Mechanics and its applications. Kluwer Publ., 2004.*

Tutor for dissertation: Ing. Miloš Müller, Ph.D.
Department of Power Engineering Equipment
Dissertation Counsellor: Ing. Jan Hujer
Department of Power Engineering Equipment
Date of dissertation assignment: 1 February 2017
Date of dissertation submission: 1 May 2018


prof. Dr. Ing. Petr Lenfeld
Dean




doc. Ing. Václav Dvořák, Ph.D.
Head of Department

Liberec, dated: 1 February 2017



Anglická verze:

Declaration

I hereby certify that I have been informed the Act 121/2000, the Copyright Act of the Czech Republic, namely § 60 - Schoolwork, applies to my master thesis in full scope.

I acknowledge that the Technical University of Liberec (TUL) does not infringe my copyrights by using my master thesis for TUL's internal purposes.

I am aware of my obligation to inform TUL on having used or licensed to use my master thesis; in such a case TUL may require compensation of costs spent on creating the work at up to their actual amount.

I have written my master thesis myself using literature listed therein and consulting it with my thesis supervisor and my tutor.

Concurrently I confirm that the printed version of my master thesis is coincident with an electronic version, inserted into the IS STAG.

Date: 26-5-17

Signature:

ACKNOWLEDGEMENT

Foremost, I would like to express my sincere gratitude to my advisor Dr. Miloš Muller for the continuous support of my master study and research, for his patience, motivation, enthusiasm, and immense knowledge. His guidance helped me in all the time of research and writing of this thesis. I could not have imagined having a better advisor and mentor for my master study.

Besides my advisor, I would like to thank my Head of department doc. Václav Dvořák for insightful comments and encouragement. I would like to thank the rest of my thesis committee Ing. Jan Hujer for inspiration and believe on me.

My sincere thanks also go to Ing. Hana Breuerová and Dr. Marek Babuška for offering me the summer internship opportunities in their company LENAM and giving me working on diverse exciting projects. I am really thankful to them to allow me to work on my thesis in their company.

I thank to my fellows in LENAM company: Martin Červa, Jakub Típek, Petr horník , Jakub Motl, Oskar Krejčí, Martin Veselý, Martin Hušek and Antonín Potěšil for the accepting me in our LENAM Family and for helping me in different situations. I thank to my friends in Technical University Liberec: Ing. Jan Novosád, Devang, Mark Lanham, Pawel Pekala and Shehab Hassan. In particular, I am grateful to Dr. Magda Vestfálová for enlightening me the first glance of research.

Last but not the least, I would like to thank my family: my parents Narendrakumar Rashiwala and Sangitaben Rashiwala, for all their sacrifices and supporting me spiritually throughout my life.

ABSTRACT

The diploma thesis is focused on the numerical and experimental analysis of cavitating flow on NACA profile 2412. The rectangular section of 150x 150 x 500 mm placed in closed loop cavitation tunnel is used for the simulation and for the measurement. The experimental profile is equipped with PVDF films used for the detection of the interaction between the cavitating flow and the profile surface. The corresponding surfaces are prepared on the numerical model to compare the force interaction. The goal of the work is to investigate the erosion potential both experimentally and numerically. The results of the flow visualization from the experiment and the corresponding flow contours in numerical analysis are compared. The erosion potential is evaluated from the number of impacts and its forces. The results of Impact forces show good agreement between the simulation and the experiment by histograms and by frequency analysis.

Keywords: Cavitation, Bubble collapse, Cavitation Erosion, NACA 2412, CFD Simulation

Table of Contents

1. Introduction	10
1.1 Introduction of Cavitation:	10
1.1.1 Vapor Pressure	12
1.2 Type of Cavitation	12
1.3 Cavitation from Hydrofoil	13
1.4 Type of cavitation from hydrofoil	14
1.4.1 Vortex cavitation	14
1.4.2 Cloud cavitation	14
1.4.3 Sheet Cavitation	15
2. Effect of cavitation and cavitating flow	16
2.1 Effect of Lift and Drag	16
2.2 Noise produced by cavitation	17
2.3 Cavitation Damage (Erosion)	18
3. Inception of cavitation	20
3.1 The role of Nuclei	20
3.2 Effect of Nuclei Size and content on cavitation inception	21
4. Current Approaches Used for Simulations of Cavitating Flow	22
4.1 Governing equations	22
4.2 Mass Transfer Models	23
4.2.1 Zwart Model	23
4.2.2 Full cavitation Model	24
4.2.3 Schnerr and Sauer Model	24
4.3 Multi-Phase model	25
4.3.1 VOF model	25
4.3.2 Mixture model	25
4.3.3 Eulerial model	26
4.4 Turbulence Models	26

4.4.1 Computational Approaches of turbulence modeling.....	26
4.4.2 The Spalart-Allmaras Model	27
4.4.3 The k-ε Turbulence Models	27
4.4.4 The k-ω Turbulence models.....	28
4.4.5 Large Eddy Simulation Models.....	28
4.4.6 V^2F Turbulent model	28
5. The description of the cavitation erosion potential	29
5.1 Physical models for description of cavitation erosion risk.....	29
5.1.1 Model by Kato et al	29
5.1.2 Model by Bark et al	31
5.1.3 Model by Fortes Patella et al	32
5.1.4 Model by Dular et al	33
5.2 Conclusion about Erosion Model	34
6. Set up the Simulation model according to the real Experiment	35
6.1 Description of real experiment.....	35
6.2 Designing model	36
6.3 Discretization of Model.....	38
6.4 Initial and Boundary conditions.....	39
7. Testing of Numerical models for cavitating flow simulations in selected regime	41
7.1 Mixture modeling approach.....	41
7.2 Selection of cavitation model.....	41
7.3 Selection of Turbulence Model	41
7.4 computation approach	42
8. Comparison of the simulations with the experiments in the cavitaiton tunnel	43
8.1 Mechanism of cavitation by Experiment	43
8.2 Mechanism of cavitation by simulation	44
8.3 Comparison of the simulations with the experiments by visualization	45

8.3.1 Inception of cavitations	45
8.3.2 Sheet cavitation	46
8.3.3 Inception of Cloud Cavitation:	46
8.3.4 Cloud cavitation	47
8.3.5 Collapse of Cloud Cavitation	48
8.4 Comparison of Simulations and experiments by PVDF films	49
8.5 Comparison of Simulations and experiments by Hydrophone.....	51
8.6 Comparison of PVDF signal and Photos of Experiment	51
8.7 Comparison between Simulation Images and Signal of pressure	54
8.8 Interested regimes.....	55
9. Comparison of frequency by simulation and by experiment	57
10. Data Analysis of impact force by Histogram	59
10.1 Data analysis for experiment.....	59
10.2 Data analysis for simulation	61
10.3 Comparison of Histogram of cavitation collapses by Experiment and by Simulation	65
11. Summary	67
12. Conclusion	69
13. Abbreviation and Nomenclature	70
14. References	72
15. Appendix	73

1 INTRODUCTION:

1.1. Introduction of Cavitation:

Cavitation can be defined as the formation and activity of bubbles or cavities within a liquid. Formation represents creation of a new cavity or to the expansion of a preexisting one to microscopic size. The bubbles may be suspended in the liquid or may be trapped in tiny cracks either in the liquid's boundary surface or in solid particles suspended in the liquid.

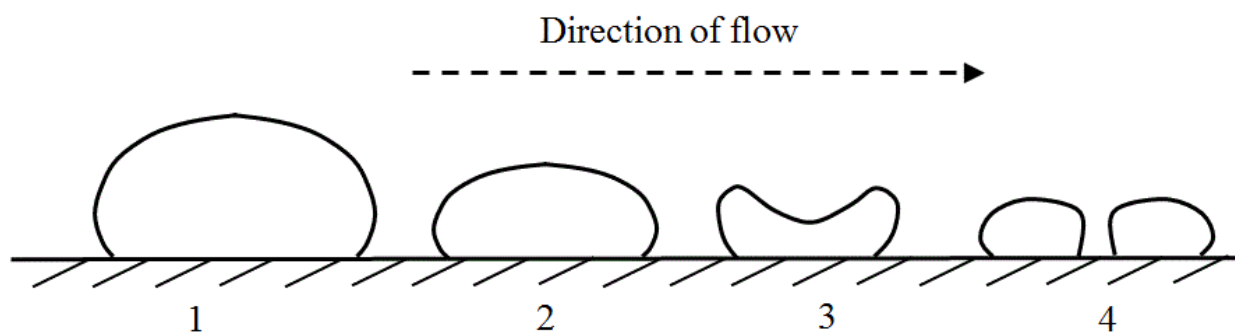


Fig 1.1 Collapse of bubble near to surface

The expansion of the minute bubbles can be caused by reducing the ambient static or dynamic pressure. The bubbles then become large enough to be visible to the eye. The bubbles may contain gas or vapor or their mixture. If the bubbles contain gas, the bubble expansion can be caused by diffusion of dissolved gasses from the liquid into the bubble by pressure reduction or by rise in temperature. If the bubbles contain only vapor, the sufficient reduction in ambient pressure at constant temperature causes an explosive vaporization into the bubbles. This phenomenon is called cavitation. The raising in temperature at constant pressure causes the grow vapor bubbles. This effect is known as boiling. This means that vaporization or boiling do not occur until the threshold are reached. [1] When the bubbles implode near to surfaces it can produce side effects causing the cavitation erosion as present in Figure 1.1

1.1.1 Vapor Pressure:

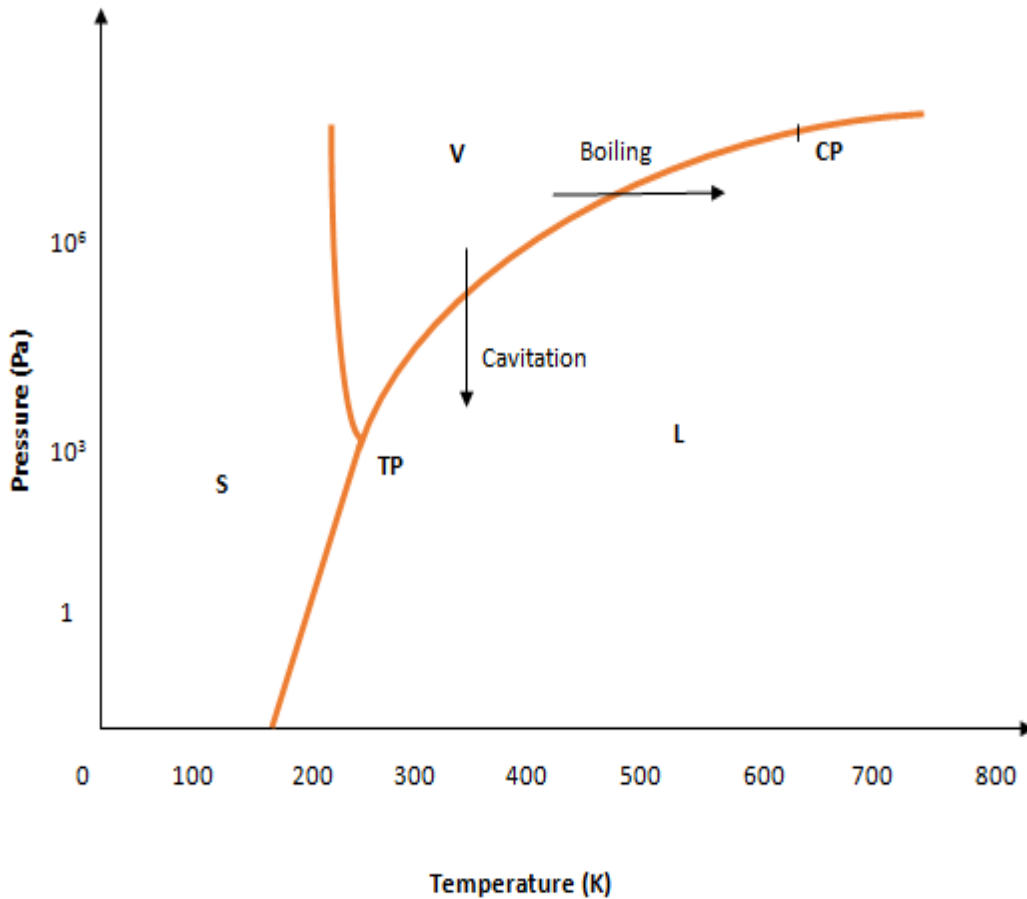


Figure 1.2 Water phase diagram

The water phase diagram can be used to understand the concept of vapor pressure. The curve from the triple point TP to critical point C separates the liquid and vapor phases. As shown in figure 1.2 crossing that phase line represents reversible transformation from one phase to another phase.

According to this, Cavitation in liquid occurs by decreasing pressure at constant temperature and Cavitation is quite similar to boiling but driving mechanism is not by changing in temperature but by changing in pressure. This pressure reduction is generally controlled by flow dynamics. [2]

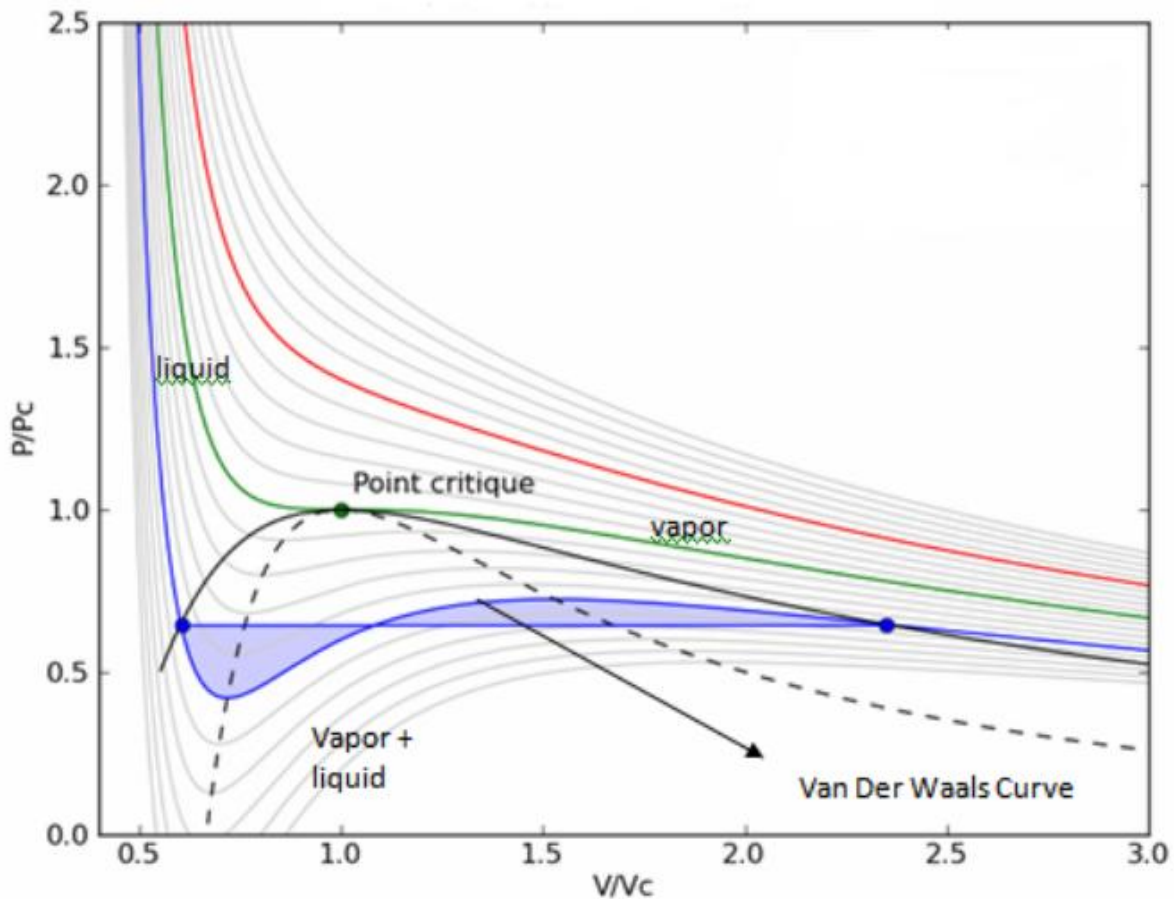


Figure 1.3 Van der Waals P-V diagram

At most of cases, the phase changes occur at the pressure which is lower than vapor pressure V_p . This can be figured by Andrew isothermals P-v diagram in figure 1.3. This curve can be approximated by van der Waals equation of state along this path, the liquid in metastable equilibrium and held in negative pressures (tensile stresses) without any phase change [11].

1.2 type of cavitation:

1. **Hydrodynamic cavitation** can be produced by pressure variations in a flowing liquid due to the geometry of the system.
2. **Acoustic cavitation** can be produced by sound waves in a liquid due to pressure variations. (Ultrasonic cavitation)
3. **Optic cavitation** can be produced by photons of high intensity (laser) light rupturing in a liquid.
4. **Particle cavitation** is produced by any other type of elementary particles, e.g. a proton, rupturing a liquid, as in a bubble chamber. (Proton, rupturing a liquid in a bubble chamber)

1.3 Cavitation from hydrofoils:

Hydrofoils are used to produce lift in boats, stabilizers, propellers, pumps and turbines. The Fig. 1.4 show that the water has to travel further round the top of the hydrofoil than the bottom. Hence it has to move faster round the top of hydrofoil, by Bernoulli's theorem, there is a pressure drop on the top of hydrofoil compared with the bottom.

Thus the lift is achieved. Both curvature of section, called camber, and operation at a positive angle of attack (the angle between the line joining the extreme end point of the hydrofoil and the horizontal) contribute to the lift. As the flow velocity is increased, the pressure drop increases and when it is greater than the available static pressure, cavitation may occur in various zones. This cavitation causes loss of lift and increased in drag. [1]

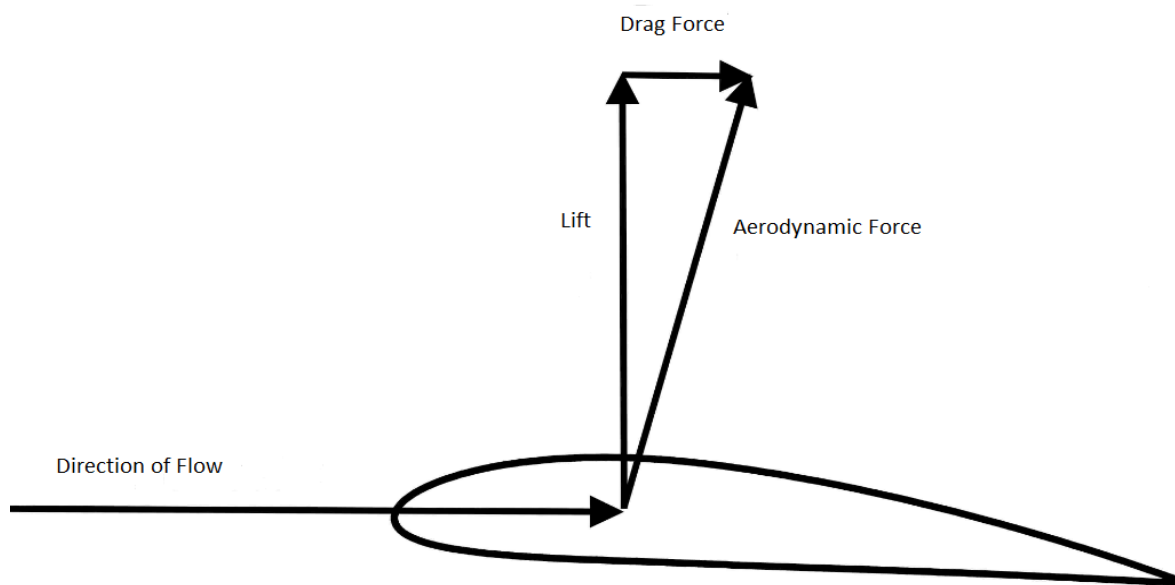


Figure 1.4: water flow around a hydrofoil creates lift

The cavitation performance can be expressed in terms of the cavitation number σ :

$$\sigma = \frac{P_0 - P_v}{\frac{1}{2}\rho u^2} \quad (1.1)$$

Where, P_0 = ambient static pressure

P_v = vapor pressure

ρ = Density of the fluid

u = velocity of fluid

1.4 Type of cavitation near to hydrofoil:

1.4.1 Vortex cavitation:

Vortex cavitation occurs due to high Reynolds number flows which contains a region of concentrated vortices, where pressure is quite smaller than in the rest of the flow. Cavitation inception often occurs in these vortices flowed by reduction of cavitation number, whole region of vortex become filled with vapor. [10]

1.4.2 Cloud Cavitation:

In many flows periodic formation and collapses of cloud of cavity bubbles can be observed. This type of structure is known as cloud cavitation. The common examples of cloud cavitation are interaction between rotor and stator blades in pump and interactions between ship's propeller and non-uniform wake created by hull. [10]

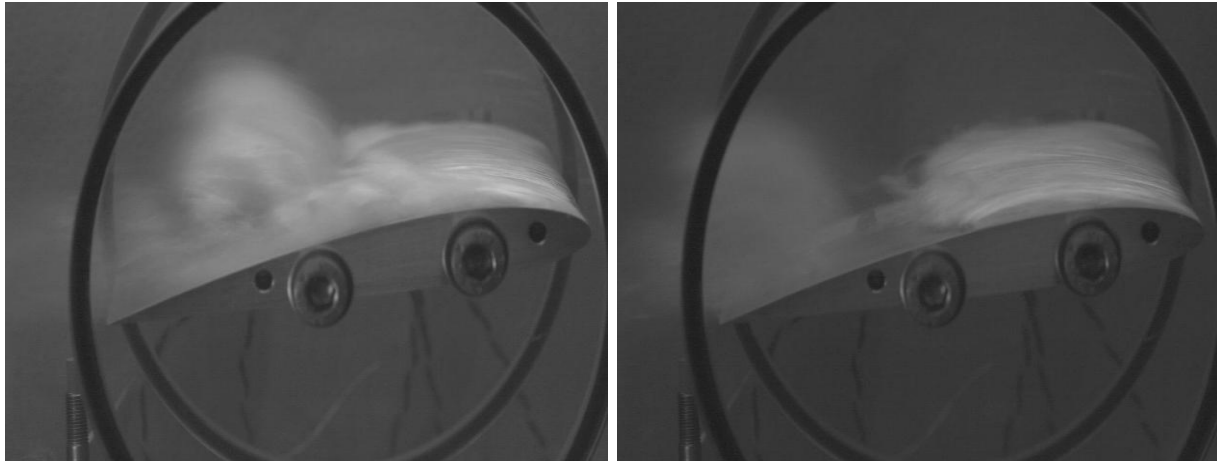


Figure 1.5: structure of cloud cavitation

Two frames in figure 1.5 shows the formation, separation, and collapse of a cavitation cloud on the suction surface of a hydrofoil. Collapses of cloud cavitation can cause more intense noise and more potential for damage than in a similar non-fluctuating flow. The collapse of cavitating cloud on hydrofoil was studied e.g. by Bark and von Berlekom, Kubota et al and Kato. [10]

1.4.3 Sheet Cavitation:

The Sheet cavitation occurs when a region of separated flow fills with vapor. At higher angle of attack, the cavitation occurs as a single vapor-filled separation. [10]

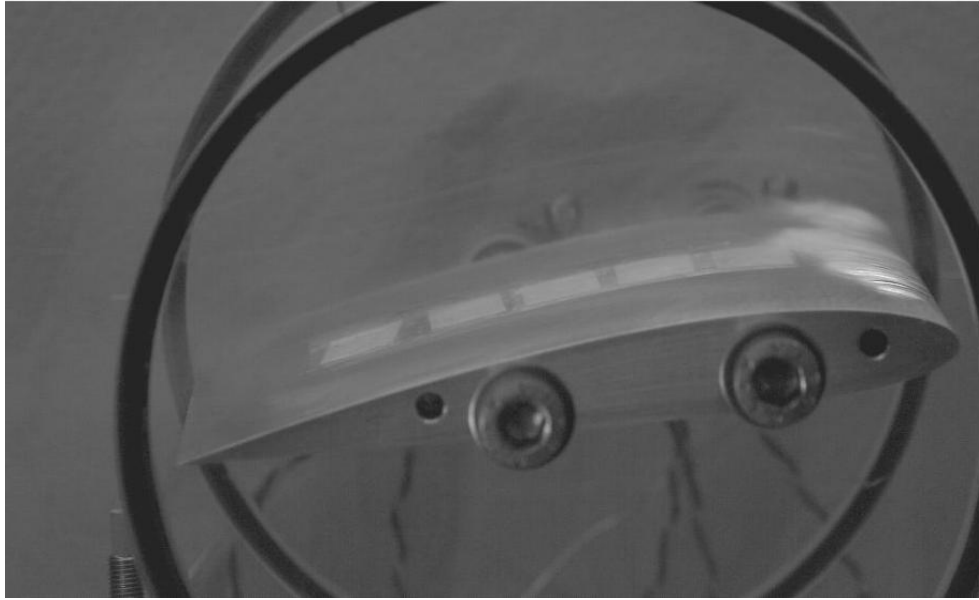


Figure 1.6: Sheet cavitation on suction side of a NACA 2412

Bluff bodies often exhibit a sudden transition from travelling bubble cavitation to a single vapor filled wake. An example of sheet cavitation is shown in Figure 1.6.

2. Effect of cavitation and cavitating flow:

2.1 Effect of Lift and Drag:

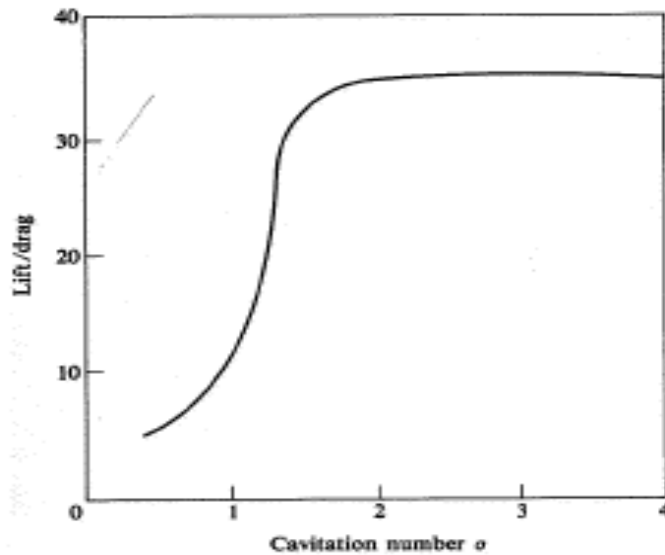


Figure 1.9: Lift/Drage vs Cavitation number [3]

Figure 1.9 shows that flow velocity increase and cavitation number decreases, the lift-drag ratio falling down sharply after certain cavitation number. Important is that lift-drag ration is highly effected by angle of attack. [3]

At constant flow speed, the lift and drag on a hydrofoil do not vary as ambient pressure is lowered but when cavitation develops, the lift decreases and drag is increases. Flow becomes unsteady and it produces vibrations in hydraulic machines.

The loss in lift can be shown by examined the pressure distribution in two figures.

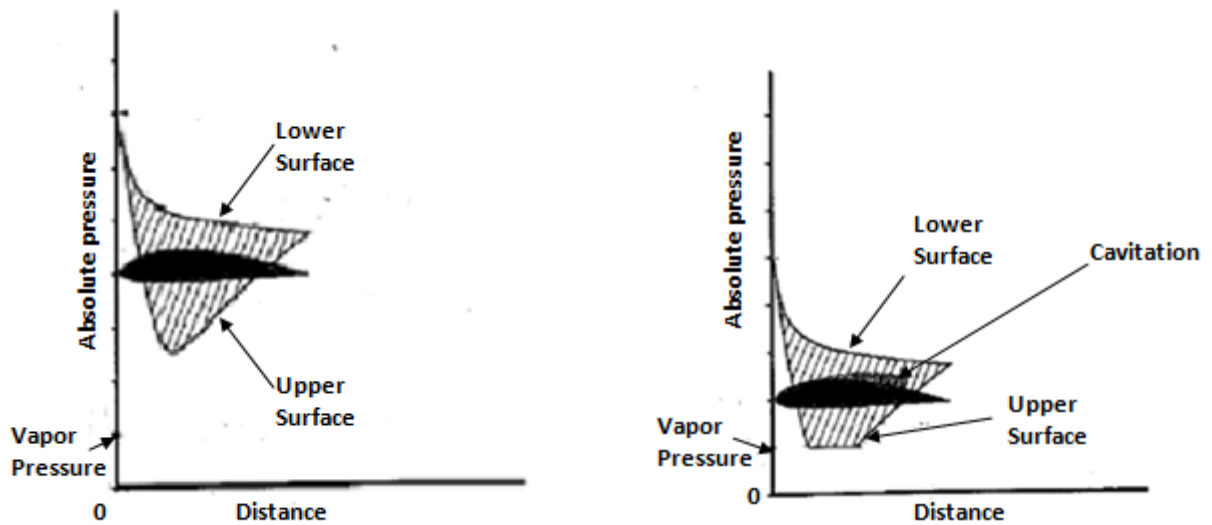


Figure 2.1: Effect of Pressure on cavitation

Figure 2.1[a] shows that the lift is proportional to the difference in the curves representing the pressure distribution on upper surface and lower surface of hydrofoil. As ambient pressure is decreases, at the same time pressures decrease at lower surface and higher surface in same quantity until cavitation begins. At this point upper surface cannot decrease below cavity pressure which is near to vapor pressure at the same time pressure decreases at lower surface, pressure drops which is shown in figure 2.1[b]. The shape of the pressure curve changes as cavitation develops the resultant pressure distribution is going to be cause as increase Drag. Due to increase in drag, Hydrofoil or some another hydraulic machines decrease efficiency in cavitation. When cavitation is unavoidable and condition are such as that supercavitation extreme flow can be assured so it is possible to use supercavitating hydro profiles which designed to get high lift-drag ratio. [2]

2.2 Noise Produced by cavitation:

Cavitation bubble collapse also produces noise in pump or any hydraulic machines. In reality, the noise is not only important because of vibration but it shows the presence of cavitation and ultimately describes cavitation damage and magnitude of cavitation itself used to measure rate of cavitation erosion. As example, Lush and Angell (1984) have shown that, in a given flow at a given cavitation number, the rate of erosion (weight loss) due to cavitation damage is depend on the noise as the different velocity of the fluid which is similar to the figure as shown as below. [3]

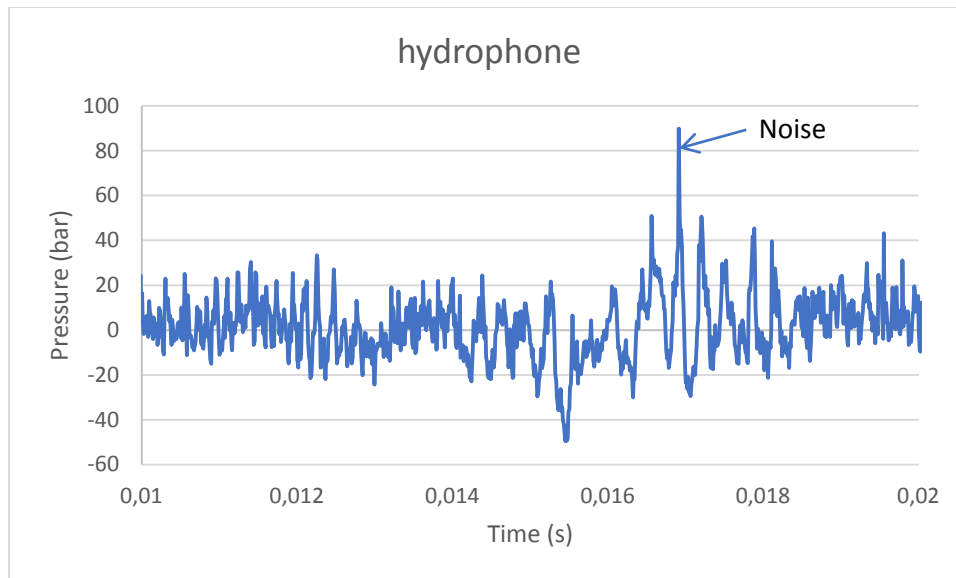


Figure 2.2: Typical acoustic signal analysis from bubble collapse which is measured by hydrophone

2.3 Cavitation Damage (erosion):

Cavitation erosion is the process of surface deterioration and surface material loss due to the generation of vapor or gas pockets inside the flow of liquid. These pockets are formed due to low pressure well below the saturation vapor pressure of the liquid and erosion caused by the bombardment of vapor bubbles on the surface. [12]

Cavitation erosion can occur on the surfaces of metals and nonmetals. It may produce undesirable noise levels and reduce the useful life of very valuable property. Noise created due to cavitation erosion in submarines increases the risk of enemy detection during wartime. In the case of pumps, cavitation erosion risks are increased by a smaller inlet pipe diameter and inlet restrictions, combined with higher liquid viscosity.

Cavitation erosion can damage and destroy critical and valuable equipment, such as industrial /military /power station equipment and parts, such as pump impellers, delicately balanced high-speed propellers and turbine blades (see in figure 2.3), causing failures leading to potential risk of life and injury for workers and others; loss of revenue, due to equipment downtime and the extra costs of failure analysis, repair and replacement.



Figure 2.3: Cavitation Erosion on Blade

3. Inception of Cavitation:

3.1 The role of nuclei:

Inception of cavitation in single or multi component liquid occurs at the pressure near to vapor pressure which contains nuclei of gas, vapor or both. When the pressure decrease nuclei become unstable, it grows and due that cavitation begins. The growth of bubble can be derived by the static equilibrium condition for sphere nuclei as shown in figure 3.1.

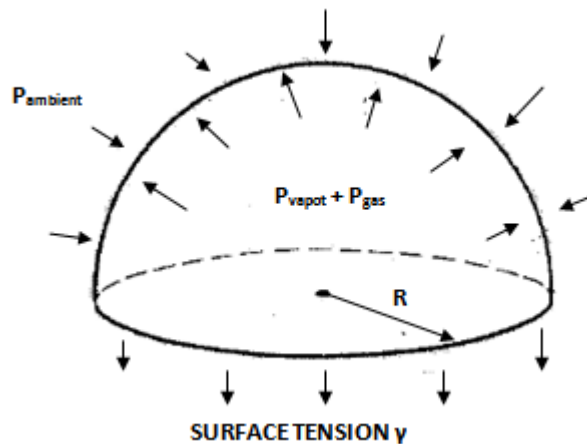


Figure 3.1: The force on cavitation bubble nucleus

The internal forces which are partial pressure of vapor and gases in nuclei are equal to the ambient pressure and surface tension between liquid and nuclei interphase. So the condition for that static equilibrium is that ambient pressure and surface tension pressure is equal to vapor pressure and gas pressure inside Bubble. [2]

$$P_a + \frac{2\gamma}{R} = P_v + \frac{const}{R^3}$$

This equation is plotted in figure for two gas contents.

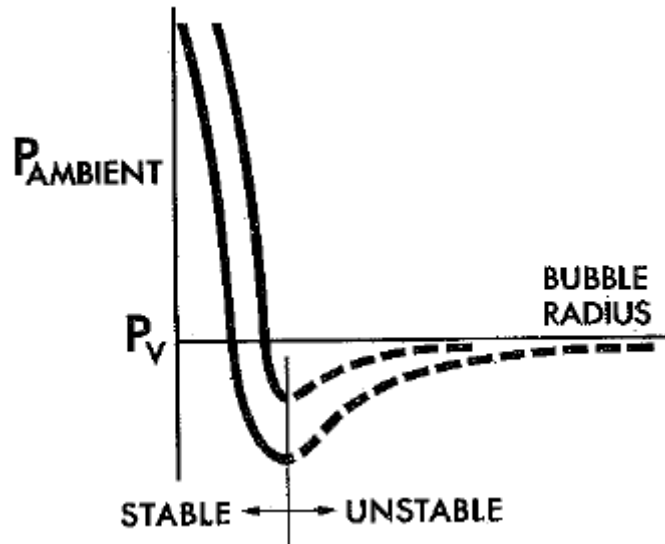


Figure 3.2: Plot of conditions for static equilibrium of cavitation bubble nuclei [2]

As shown in figure 3.2, the pressure adjacent to bubble is lower value which below than vapor pressure of the water. And Bubble has tendency to increase pressure which above that minimum, so initial bubble is smaller than current bubble size. And it said to be nuclei in stable condition and it stable till it has been reached to the equilibrium radius as left portion of the curve where slope is negative. If the pressure drop below than its critical value, bubble is going to be unstable and it growth without any bound. [2]

3.2 Effect of Nuclei Size and content on cavitation inception:

Stable nuclei can be smaller in size which is disappears in time due to gas or vapor content diffuses into Surrounding fluid. So, greater pressure reduction required to cause cavitation in any hydrodynamic system. It can be understand by an example.

The venture experiment is done by Phillips Eisenberg who is comparing cavitation inception pressure for fresh drawn water with that water which undisturbed rested for some time. Increasing in pressure head is meant to directly increasing velocity to atmosphere and due to that increasing static pressure at throat. With freshly drawn tap water, cavitation begins at pressure head at 2 feet, and it develops more cavitation with increasing pressure head. After leaving the water undisturbed for 1 hour and repeating experiment, it shows that it required higher pressure head for inception of cavitation. So we conclude that during setting period some nuclei could rise to surface and vent if there are really large but some could decrease in size due to diffusion of air in liquid. [2]

4. Current Approaches Used for Simulations of Cavitating Flow:

The bubble dynamic equation presented by Plesset as shown in equation 4.1 . All cavitation models based on the Rayleigh-Plesset equation have been applied, whose differences are focused in the condensation and vaporization process. The bubble dynamics equation can be derived from the generalized Rayleigh-Plesset equation as

$$R_b \frac{D^2 R_b}{Dt^2} + \frac{3}{2} \left(\frac{DR_b}{Dt} \right)^2 = \left(\frac{P_b - P}{\rho_l} \right) - \frac{4v_l}{R_b} R_b - \frac{2\sigma}{\rho_l R_b} \quad (4.1)$$

Where,

R_b = bubble radius

σ = liquid surface tension coefficient

ρ_l = liquid density

P_b = bubble surface pressure

P = local field pressure.

The Rayleigh-Plesset equation is the basis in the area of numerical investigations, which covered the analyses of behavior of a single bubble under the influence of the variable pressure of the surrounding liquid. In the course of time, the focus of research works on cavitation has changed. The place of the analyses of the behavior of a single bubble was taken by the cavitating flow considered as a whole. All numerical simulations of the cavitating flow, regardless of the used approach (multi-fluid or homogeneous), require solving the appropriate set of governing equations, which include mass, momentum or energy equations. [5]

4.1 Governing Equations:

In the homogeneous multiphase transport equation based model, the cavitating flow is described by following equations:

$$\nabla \cdot U = \dot{m} \left(\frac{1}{\rho_l} - \frac{1}{\rho_v} \right) \quad (4.2)$$

$$\frac{\partial(\rho U)}{\partial t} + \nabla \cdot (\rho U U) = -\nabla P - \nabla \cdot \tau + S_M \quad (4.3)$$

$$\frac{\partial \gamma}{\partial t} + \nabla \cdot (\gamma U) = \frac{\dot{m}}{\rho_l} \quad (4.4)$$

Cavitating flow is considered as a Mixture of two phases i.e. Vapor and liquid behaving as one flow. The phases are considered incompressible and share the same instantaneous velocity U and pressure P . The derivation of these equations can be found in Zwart et model.

The above equations are in order, the continuity and the momentum equation for liquid-vapor mixture, and the volume fraction equation for the liquid state. τ is the stress tensor, S_M stays for additional sources of momentum (for instance the Coriolis and centrifugal forces in the rotating frame of reference), \dot{m} is the interphase mass transfer rate due to cavitation, ρ_v the vapor density, ρ_l the liquid density.[5]

$$\gamma = \frac{\text{volume liquid}}{\text{total volume}} \qquad \alpha = \frac{\text{volume vapor}}{\text{total volume}}$$

And these values are related to each other through the following relevant constitutive relationship:

$$\gamma + \alpha = 1$$

Finally, ρ and μ are the density and the dynamic viscosity of the vapor-water mixture, scaled by the water volume fraction respectively,

$$\rho = \gamma\rho_l + (1 - \gamma)\rho_v \qquad (4.5)$$

$$\mu = \gamma\mu_l + (1 - \gamma)\mu_v \qquad (4.6)$$

The specific interphase mass transfer rate \dot{m} can be solved using an appropriate mass transfer model, also called cavitation model.

If the turbulent flow is modeled using the RANS approach, in the above equations U and P stands for the statically averaged velocity and pressure fields respectively. Moreover, in the Momentum equation additional Reynolds stress terms appears. These terms can be modeled using an eddy viscosity approach such as $k-\varepsilon$ or SST turbulence model, or using a second moment closure model such as the RSM turbulence model.

4.2 Mass transfer Models:

Mass transfer model is called as cavitation model and this model accounts mass transfer from single liquid to its vapor. In the following, we describe about three different mass transfer models compared in study, where the interphase mass transfer rate due to cavitation was assumed positive if directs from vapor to water.

4.2.1 Zwart Model:

The Zwart model is the native CFX mass transfer model. It is based on the simplified Rayleigh-Plesset equation for bubble dynamics in 1955 by Brennen:

$$\dot{m} = \begin{cases} -F_e \frac{3r_{nuc}(1-\alpha)\rho_v}{R_b} \sqrt{\frac{2}{3} \frac{P_v - P}{\rho_l}} & \text{if } P < P_v \\ F_c \frac{3\alpha\rho_v}{R_b} \sqrt{\frac{2}{3} \frac{P - P_v}{\rho_l}} & \text{if } P > P_v \end{cases} \quad (4.7)$$

In the above equations, P_v is the liquid vapor pressure, r_{nuc} the nucleation site volume fraction, R_b the radius of nucleation site, F_e and F_c are two empirical calibration coefficients for the evaporation and the condensation processes respectively. In CFX the above mentioned coefficients by Defaults, are set as follow: $r_{nuc} = 5$, [5]

Moreover, from above equations it can be seen that expressions for condensation and evaporation are not symmetric. In particular, it is possible to recognize that in the expression for evaporation α is replaced by $r_{nuc} (1 - \alpha)$ to take into account that, as the vapor volume fraction increases, the nucleation site density must decrease accordingly.

4.2.2 Full cavitation Model:

The mass transfer model proposed by Singhal et al originally known as full cavitation model, is currently employed in some commercial CFD codes, for instance FLUENT and PUMPLINX. This model is also based on the reduced form of the Rayleigh-Plesset equation for bubble-dynamics and its formation states as follows, where f_v is the vapor mass fraction, k the turbulence kinetic energy, T the surface tension, $C_e=0.02$ and $C_c=0.01$ are two calibration coefficient.[5]

$$\dot{m} = \begin{cases} -C_e \frac{\sqrt{k}}{T} \rho_l \rho_v \sqrt{\frac{2}{3} \frac{P_v - P}{\rho_l}} (1 - f_v) & \text{if } P < P_v \\ C_c \frac{\sqrt{k}}{T} \rho_l \rho_l \sqrt{\frac{2}{3} \frac{P - P_v}{\rho_l}} f_v & \text{if } P > P_v \end{cases} \quad (4.8)$$

Where, f_v = vapor mass fraction.

4.2.3 Schnerr and Sauer Model:

Schnerr and Sauer Model has similar approach as full cavitation model. It uses the following expression give relation between the vapor volume fraction and number of bubbles per volume of liquid. [5]

$$\alpha = \frac{n_b \frac{4}{3} \pi R_b^3}{1 + n_b \frac{4}{3} \pi R_b^3} \quad (4.9)$$

Where,

α = vapor volume fraction,

n_b = number of bubbles,

R_b = radius of bubble.

In this model, unlikely from other two models, implementation is the number of spherical bubbles per volume of liquid. If you assume that no bubbles are created or destroyed, the bubble number density should be constant as $\alpha=0$ and $\alpha=1$. The initial conditions for the nucleation site volume fraction and the equilibrium bubble radius would therefore be sufficient to specify the bubble number density and phase translation which is shown as below.

$$\dot{m} = \begin{cases} \alpha(1 - \alpha) \frac{3}{R_B} \frac{\rho_l \rho_v}{\rho} \sqrt{\frac{2}{3} \frac{P_v - P}{\rho_l}} & \text{if } P < P_v \\ \alpha(1 - \alpha) \frac{3}{R_B} \frac{\rho_l \rho_v}{\rho} \sqrt{\frac{2}{3} \frac{P - P_v}{\rho_l}} & \text{if } P > P_v \end{cases} \quad (4.10)$$

There are many different cavitation models but basically we used above three Models which is implemented in ANSYS FLUENT.

4.3 Multi-phase models:

All multi-phase models work on the Euler-Euler approach. In this approach, different phases are treated as interpenetrating continua. Here, the volume fractions are assumed to be continuous function of space and time. And sum of both quantities is equal to one. Conservation equations for each phase used to get set of equations, which are similar for all phase. These equations give exact constitutive relations which are obtained from empirical information or by application of kinetic energy. Information of different type of Multi-phase models is given as below.

4.3.1 VOF model:

The VOF model is about surface tracking technique which applied to fixed Eulerian mesh. It is designed for two or more immiscible fluid where position of interface between two phases is point of interest. The main point of VOF model is that a single set of momentum equations is shared by the fluids and the volume fraction of each fluid in each computation cell is tracked throughout the whole domain.

This model is used to describe Stratified flow, free-surface flow, filling, sloshing, and motion of large bubbles in liquid, the motion of liquid after dam break, prediction of jet surface tension and steady or transient tracking of any liquid-gas interface. This model doesn't allow for void regions where liquid is not present and allows only for one of phases which can be defined as compressible ideal gas. [8]

4.3.2 Mixture Model:

Mixture Model is a simplified multiphase model than is used to model multi-phase flows where the phases move at different velocities. The coupling between the phases should be strong and it can also be used to model homogeneous multiphase flows with very strong coupling and phases are moving

at same velocity. Mixture can be used to calculate non-Newtonian viscosity. This model is considered as model n phases by solving momentum, continuity and energy equation for mixture, volume fraction, and equation for secondary phases and algebraic expression for relative velocities.

This model is also applicable for liquid-solid flow, and this model has some advantages over VOF model. 1. It allows the phase to be interpenetrating and 2. It allows phases to move at different velocity using concept of slip velocities.[8]

4.3.3 Eulerial Model:

Eulerial model allows for modeling of multiple phases which are separate but still interact with each-other. It is most complex model compare to other models; it solves a set of n momentum and continuity equations for each phase. Coupling between phases can be obtained by the pressure and interphase exchange co-efficient. This coupling works differently as different phases involved. For granular flows, the properties are obtained from application of kinetic theory and momentum exchange between phases are depends on type of mixture used for the model. [8]

Application of this model includes bubble column, riser, and particle suspension and fluidized beds.

4.4 Turbulence Model:

Study about the behavior of Fluid is really necessary to get to know effect of cavitation near to hydrofoil. Turbulence Model is based on Navier-Stoke Equations which govern pressure and Velocity of the Fluid. Turbulence is unsteady and irregular motion in which transported quantity like mass momentum fluctuate in time and space. The k- ω and SST k- ω models are more appropriate for this experiment which discussed later.

4.4.1 Computational Approaches of turbulence modeling:

Reynolds-Averaged Navier-stokes model:

This model can solve ensemble-averaged Navier-stokes equations. These models are mostly used for calculating industrial flows and benefit of this model is to solve all turbulence length scale. [8] RNS based models are spalart – allmaras model, two equation model, standard k- ϵ model, RNG k- ϵ model, Realizable k- ω model, standard k- ω model, SST k- ω model, Reynolds stress model in FLUENT.

Large Eddy Simulation:

It solves the spatially averaged Navier-Stokes equations. Large eddies are directly resolved but eddies smaller than the mesh are modeled.[8] It is less expensive than DNS but the amount of computational resources and efforts are needed for most practical applications.

Direct Numerical Simulation (DNS):

Theoretically all turbulent flows can be calculated or simulated by numerically solving full Navier-Stokes equations and it resolves the whole spectrum of scales and no modeling is required. [8] It is a time-consuming process so it is not used in industrial application or neither in FLUENT.

4.4.2 The Spalart-Allmaras Model:

The Spalart-Allmaras model is a low-cost RANS model which only considers a transport equation for modified eddy viscosity. This model is in modified form so the eddy viscosity is easily resolved near to the wall. This model is mainly used for aerodynamics and turbo-machinery applications, such as supersonic flow over airfoil, boundary-layer flow etc. [8]

This model embodies a relatively new class of one equation model where it is not necessary to calculate a length scale related to local shear layer thickness. And it is designed specifically for aerospace fields involving wall-bounded flows. But this model is still relatively new.

4.4.3 The k-ε Turbulence Models:

1. Standard k-ε model:

Standard k-ε model is the most widely used engineering turbulence model for industrial application. It contains sub-models for compressibility, buoyancy, combustion etc. But it has some limitations. The ε equation contains a term which cannot be calculated at the wall. Therefore, wall functions have to be used and it does not work properly for flows with strong separation, large streamline curvature and larger pressure gradient. [8]

2. Renormalization group (RNG) k-ε model:

Renormalization group k-ε model has a constant which is derived from renormalization group theory. This model contains a differential viscosity model from low Reynolds number (Re) effects, algebraic formula for Prandtl number or Schmidt number and swirl modification. It performs better than standard k-ε model for complex flow with swirl. [8]

3. Realizable k-ε (RKE) model:

Realizable k-ε model is consistent with physical turbulent models but it also satisfies certain mathematical constraints as follows:

Positivity of normal stresses: $\overline{u'_i u'_j} > 0$

Schwarz inequality for Reynolds shear stress: $(\overline{u'_i u'_j})^2 \leq \overline{u'^2_i} \overline{u'^2_j}$

This model gives accurate details of spreading rate of both planar and round jets. And it shows effective performance under strong adverse pressure gradients, separation and recirculation. [8]

4.4.4 The k- ω Turbulence models:

The k- ω model is more effective or useful compare to k- ϵ models because it integrated to the wall without using any wall function. And this model is more accurate and robust for wide range of boundary layer flows with pressure gradient. There are two types of k- ω model in FLUENT.

1. **Standard k- ω model:**

Standard k- ω model is widely used in Aerospace and turbo-machinery applications. It has some sub-models like compressibility effects, transitional flows and shear floe correction.

2. **Shear stress transport k- ω model:**

This model uses blending function to gradually convert from the standard k- ω model near the wall to high Reynolds number version of k- ω model in outer portion of boundary layers. And it has to modify turbulent viscosity formulation to consider effect of principle turbulence shear stress. [8]

4.4.5 Large Eddy Simulation models:

Large eddy simulation model is more accurate over RANS model. This model uses in such application like combustion, mixing and external Aerodynamics.

This model is implemented in FLUENT in two different models due to different consideration.

1. Sub grid scale turbulence models;
2. Detached eddy simulation model.

This model is applicable to all combustion model in FLUENT and this model has statistic tools like Time averaged and RMS values of solution variables, built-in fast Fourier Transformation. [8]

4.4.6 V^2F Turbulent model:

This model is developed by Paul Durbin's group. And they suggest that wall-normal fluctuation \bar{v}'^2 responsible for near wall damping of eddy viscosity. This model is used two additional transport equations for \bar{v}'^2 in which relaxation factor f to be solve together with k and ϵ . and V_T depends on $\bar{v}'^2 T$ instead of kT .

This model can be used for 3D problem, low Reynolds number and for boundary layer. It improves prediction for heat transfer in jet impingement and separation flow where k- ω model does not work. It is still eddy viscosity model so it has some limitations. [8]

5. The description of the cavitation erosion potential:

Description of the cavitation erosion is a post-processing procedure for understand of cavitation erosion potential based on multiphase CFD result which compared with experimental result. Here it is necessary to get connection between the available information that comes from RANS and experimental observations with high speed camera.

5.1 Physical models for description of cavitation erosion risk:

These all cavitation erosion model gives brief information about physical processes from cavity micro-structure to bubble cloud collapses. And this models are developed to understand erosion phenomena which happed by cavitation by CFD result and by Experiment observation. There are four different erosion models which are published by Tom j.c.Terwisga in Michigan USA.

1. Kato et al.
2. Bark et al.
3. Fortes Patella et al.
4. Duller et al.

5.1.1 Model by Kato et al. (1996)

In this model, it describes quantitative prediction of impact force distribution or pressure distribution on solid surface which is caused by cavitation. In this model, it is assumed that the shock wave generated by the collapses of bubbles which are separated from sheet cavity. This whole procedure describe in six stages which are given below.

Stage 1: Cavity type and extent

Stage 2: Cavity generation rate

Stage 3: Number and size distribution of cavity bubbles

Stage 4: Characteristics of collapse bubbles

Stage 5: Impact force on solid wall due to bubble collapses

Stage 6: Amount of erosion caused by successive impact force or pressure distribution

Here, the estimation of impact force distribution or pressure spectrum is Key to prediction of cavitation erosion. This quantity can be measured and co-relate with pit -distribution. The cavity generation rate is derived from measurement of air flow rate into vapor cavity which is similar to natural cavitation including the shedding of cloud cavitation. [4]

It is difficult to measure the number and size of distribution of cavity bubbles because size of bubbles is fluctuating. But number and size of distribution of cavity bubbles can be recognize by a measurement of air bubble distribution. Down-steam of cavity collapse region because bubbles are remains same in down-steam as shown in figure 5.1. It is considered that diffusion of gas in bubble negligible due to short period of time.

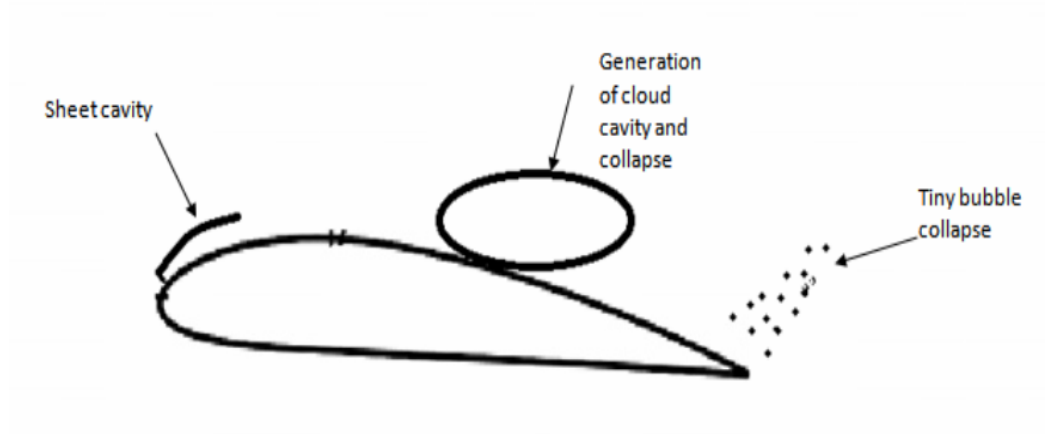


Figure 5.1: Generation and collapse of cloud cavity

Here, the pressure or impact force spectrum is analyzed from bubble generation rate and number and size of the bubbles. For that it is necessary to know in which region cavity collapse occurs. Then bubble collapse rate on specific position of surface is estimated by spatial distribution method. But it is very time consuming process to find pressure by each collapse of bubble. [4]

So it is assumed the bubble which causes impact force and pressure under effective layer which enough to damage surface. This effective layer can be represented as reference trajectory which shown is below figure 5.2.

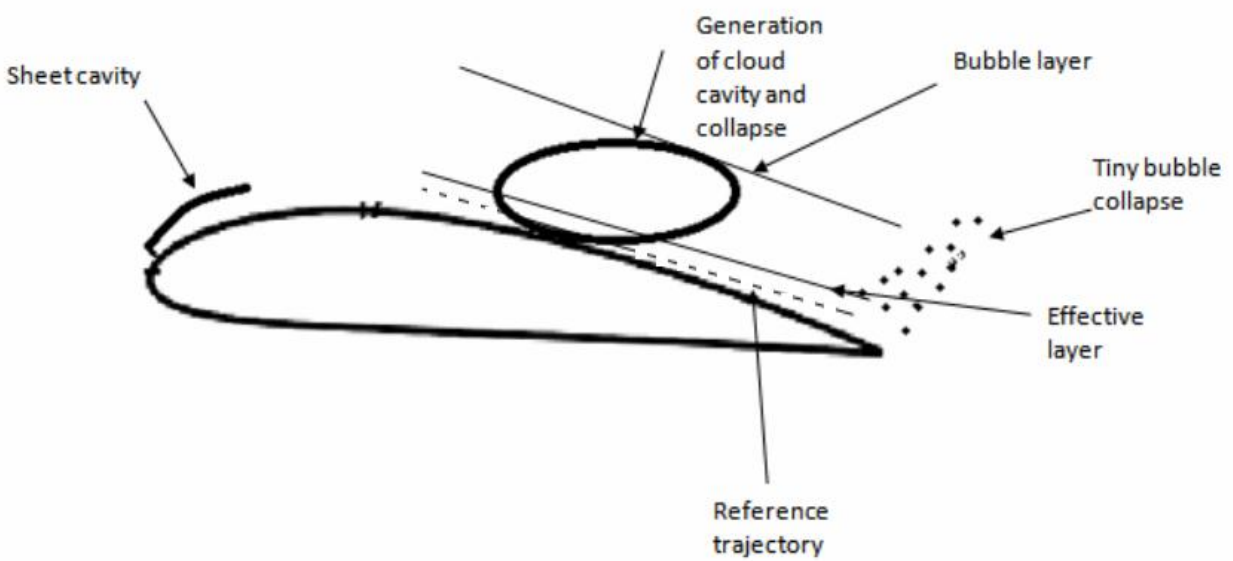


Figure 5.2 Bubble Layer, effective layer and reference trajectory

Due to this cavitation erosion can be predict without using Model test, but it is necessary to assume or neglect some parameters like initial pressure inside bubbles , interaction of bubbles each other ambient pressure near to bubbles and distribution of bubbles. [4]

This model is include generation of shock wave and give information of cavity shedding up. And this model uses some simple empherical equations which derived by experiment on only by one configuration, so it can be merely use for Propeller and Rudder analysis.

5.1.2 Model by Bark et Al. (2004):

This model shows better look in whole hydrodynamic process and gives detail information about development of erosion cavity to collapses. The model indicates that erosion is the result of accumulated energy transfer from cavity to collapsing cavity near to the surface. A working principle of this model is that works with sharp visual interpretation of observation of cavitation by high-speed camera and it can be described by the behavior of cavitation respect to generation of erosion.

The small cavities show pitting of material due to small diameter of bubbles collapses. This bubbles are considered as spherical shape as initial stage than if it comes close to surface, it transfers to micro speed jet which hitting the surface. With speed jet, local pressure is created on surface with cause deformation and fatigue of material. The effect is more curious when the collapses occur in cloud of cavity.

In cloud cavitation, cascading energy transfer from peripheral bubbles to innermost bubbles where collapse energy is in very small volume and it gives full description of decomposition of erosion cavitation process. At first to create transient flow in model and create cavity on propeller blade and main focus is collapse. The motion can be visualized by speed camera.

Bark et al model provides some guidelines to analysis erossiveness from observation. These guidelines mainly are discussed from early development to its rebound. This model is used where large-scale cavities which can be predicted by CFD method. It is very difficult when low-scale cavitation occurs and complex due to cavity behavior. This method is quite expensive and time consuming due to high speed video recording and analysis. Result are sometime overestimated or underestimated due to scale cavitation. [7]

5.1.3 Model by Fortes Patella et al:

Fortes patella et al model describes the mechanism of cavitation erosion. It shows how to measure the energy transfer from cavitating flow to the surface of material. It includes the collapse of vapor bubble in flow emission and propagation of pressure waves and its nearer solid surfaces. And damage of material exposed to pressure wave impact. [6]

This model is similar to Brak et. el model. Here potential power transforms from micro cavity and converted into acoustic power which is produced by collapsing clouds of micro-bubbles. It means pressure waves are main source contribution to Erosion. And Pressure wave integrates with near solid surfaces and produces damage on surface of material. Development of cavities can be observed by experiment or by CFD. By this model, it is easy to calculate volume damage rate. The procedure is given as below

1. To find Instantaneous Potential power:

This power is derived from macroscopic cavity structure.

$$p_{pot} = \Delta P \left(\frac{dv_{vap}}{dt} \right) \quad (5.1)$$

Where $\Delta P = P_{\Phi} - P_{vap}$

P_{Φ} = surrounding pressure

P_{vap} = vapor pressure.

2. To find flow aggressiveness potential power:

It is derived from instantaneous potential power which relates with flow aggressiveness before collapse occurs.

$$P_{pot}^{mat} = \eta^{**} P_{pot} \quad (5.2)$$

Where the energy transfer efficacy is a function of the hydrodynamic characteristics of main flow and distance n=between collapse center and material surface.

Here, flow aggressiveness power depends on unsteady flow geometry of cavitating flow angle of attack and shape of Hydrofoil.

3. Pressure Wave Power:

It is power which applied to material due to the vapor collapses.

$$P_{waves}^{mat} = \eta^* P_{pot}^{mat} \quad (5.3)$$

Where, efficiency η^* is defined by collapse of gas and vapor. It depends on surrounding pressure and air content in flow.

4. Volume damage rate:

It is measured by a 3D laser profilometer which compare to flow aggressiveness and it shows as below.

$$V_y = \frac{\eta^*}{\beta} \cdot \frac{P_{pot}^{mat}}{\Delta S} \quad (5.4)$$

Where,

ΔS = analzed sample surface

β = mechanical transfer function depends on material characteristics.

Advantages of this Model:

The benefit of this model is that it works on physical energy transfer processes. This model is highly reliable because it depends on assessment of two efficiencies. Energy transfer ratio is very important factor for interpretation of CFD model and this transfer ratio describe effectiveness of this model.

5.1.4 Model by Dular et al (2006);

This model is based on damage caused when a bubble collapse near to the solid surface. These singles bubbles are excited by the shock wave which produced by the cloud cavity. This model partly based on theory and party on empirical consideration which derived from different erosion model which are discussed before.

It is similar as old models which co-relate between the cavitation structures and cavitation erosion by experimental observation and statistical calculation. Most important assumption is that the value of standard deviation at gray level for each point relate with magnitude and distribution of damage caused by erosion.

It is divided in four phases as: 1 Collapses of cavitation cloud cause a shock wave 2. The magnitude of shock wave consider as distance from solid surface 3. Due to single bubble collapse near to wall, micro-jet wave effect on surface of model. 4. Due to jet impact, single pitting (damage) occurs on the Surface.

Here, magnitude of emitting pressure relate with velocity of collapse to the surrounding pressure from acoustic theory, Amplitude of emitted pressure is proportional to square root of acoustic pressure. So that change in cloud volume on hydrofoil depends on mean distribution of pressure wave which is produced by collapses.

In this Model, on basis of hypothesis, Dular added the instantaneous change of cavitation cloud volume by standard deviation of gray level in experiment observations which related to pressure wave. This model is still in doubt because it is reverse of the physical hypothesized process in which one implosion synchronizes the implosion of cloud cavitation. In other comment it shows that erosion aggressiveness is based on the notation that damage occurs due to jet wave by the individual bubble implosion. [7]

5.2 Conclusion about Erosion models:

At the conclusion, Bark and Fortes models are better compare to others due to easy concept and it is based on energy transfer and it gives detail information about collapses. Where, Kato model does not give detail information except energy transfer. And Dular at al model is still in doubt to use.

6 Setup the simulation model (CFD) according to the Real experiment on the Cavitation Model:

6.1 Description of real experiment:

The numerical simulations were realized based on a real experiment performed in the cavitation tunnel. The experiment was realized in Hydraulics Research Centre, Ltd. in Lutin. The boundary conditions for the CFD simulation were set according to the setup of the experiment. The measured volumetric flow rate and the inlet and outlet pressure were used for the numeric simulation setting.

The measurement section of the cavitation tunnel in Hydraulics Research Centre is shown in Figure 6.1. The figure shows the measured profile with PVDF films and needle hydrophone. The profile angle is adjustable to simulate different flow regimes. And schematic diagram of the cavitation tunnel is shown in Figure 6.2.

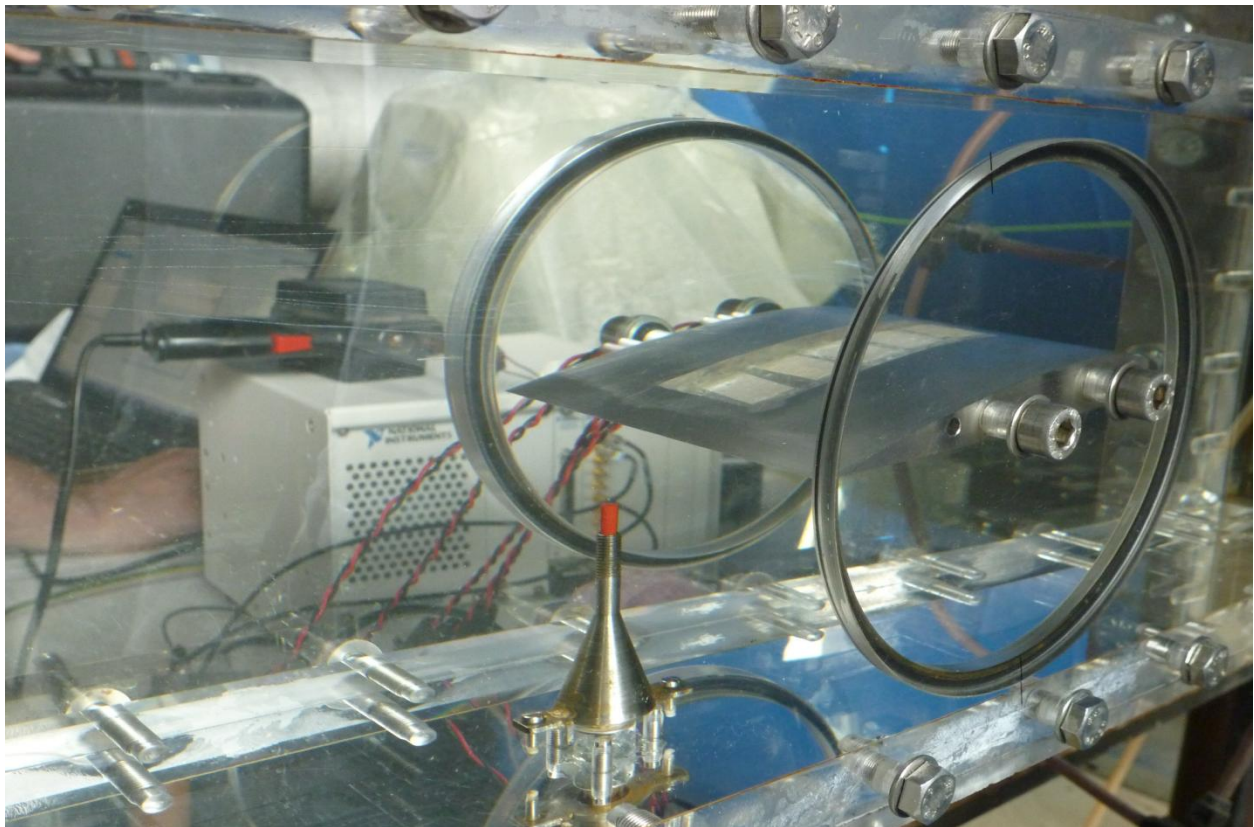


Figure 6.1: Cavitation Tunnel

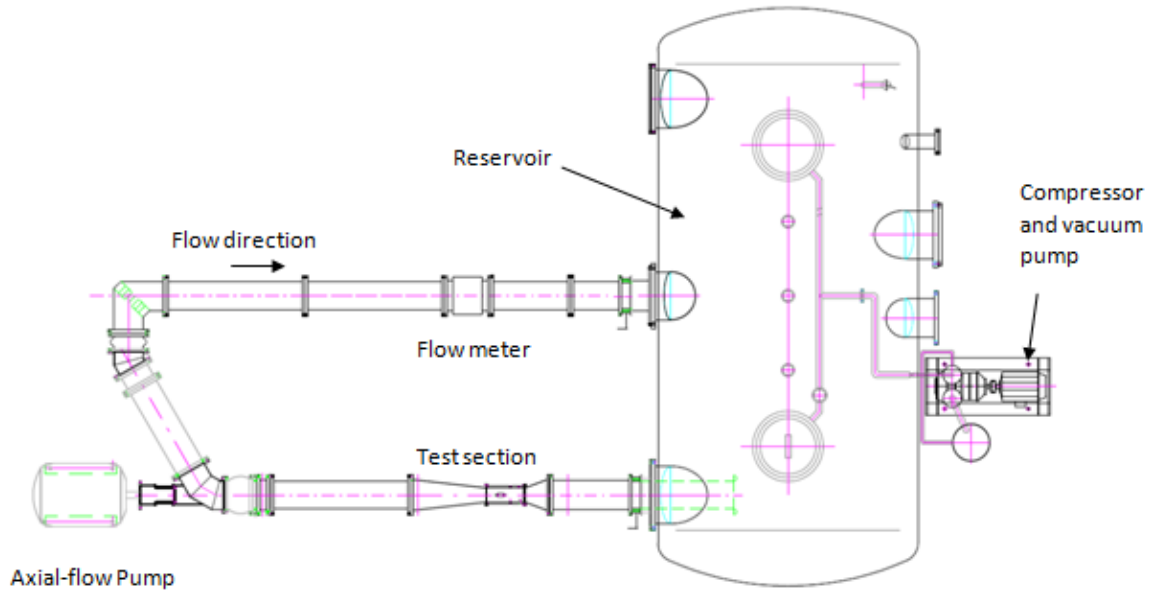


Figure 6.2: schematic diagram of the cavitation tunnel in closed water loop

The test section area is made of organic glass. The dimensions of test section are 150×150×500 mm. The flow is supplied by axial flow pump. The maximum velocity which can be reached in the section is around 25 m/s. NACA 2412 hydrofoil was used for the investigation of cavitating flow. It is prismatic profile with cord length 120 mm and span-chord ratio 1.25. The incidence angle can vary from 0 to 180 degree. For the tested regime it was set to 8 degree.

The selected regime which was used for the comparison with the numerical simulation exhibited developed cloud cavitation. The regime included following parameters:

Inlet pressure = 245 kPa,

Outlet pressure = 100 kPa

Initial flow rate = 295 lt/min

Inlet velocity = 13 m/s due.

High speed camera was used to record the cavitating flow during the experiment from the side. The recorded frequency is 1000 fps. The camera records and the PVDF film measurement are synchronized.

6.2 Designing Model:

Pro-E software is used to design the model of NACA 2412 profile. Data of NACA 2412 profile is taken from Airfoil tools website [13] (Figure 6.3.).

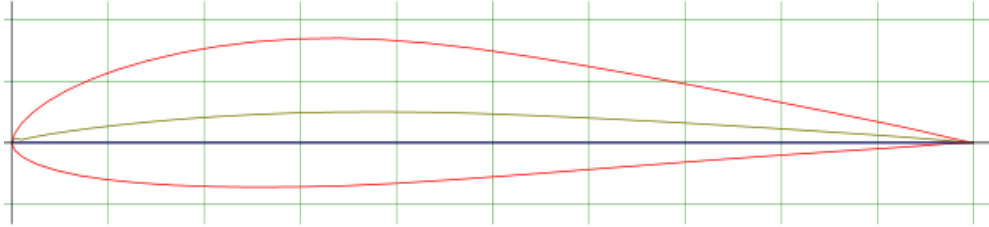


Figure 6.3: Model of NACA series 2412(13)

Dimension of test section is 150×150×500 mm, and angle of attack of blade is 8 degree. The model of the test section is shown as below in figure 6.4.

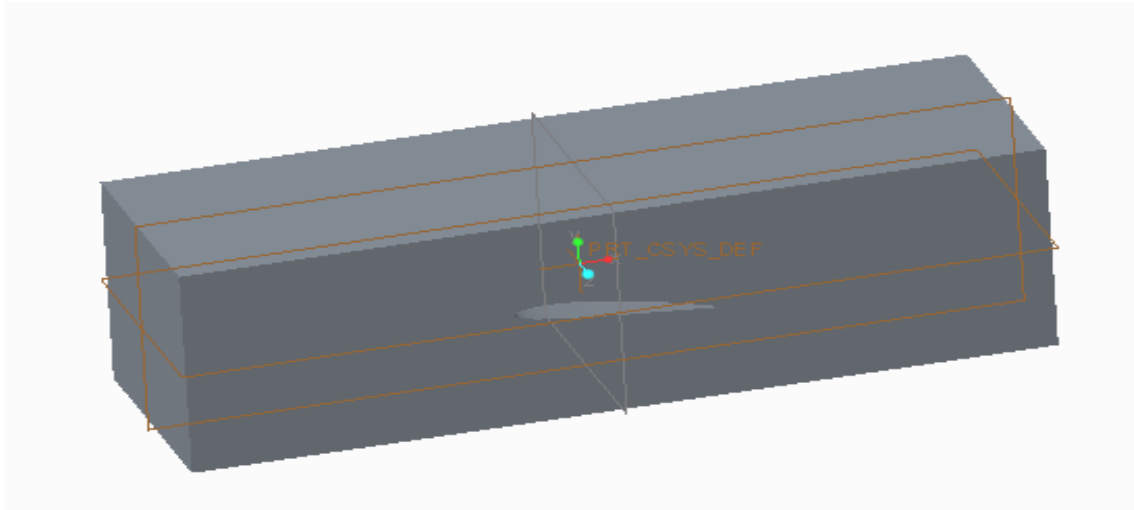


Figure 6.4: Model of test section

The installations of the PVDF films on the experimental profile and the profile used for the numerical simulation are shown in Figure 6.5. The PVDF films in the experiment are calibrated by drop ball test to provide the information about force at the location.

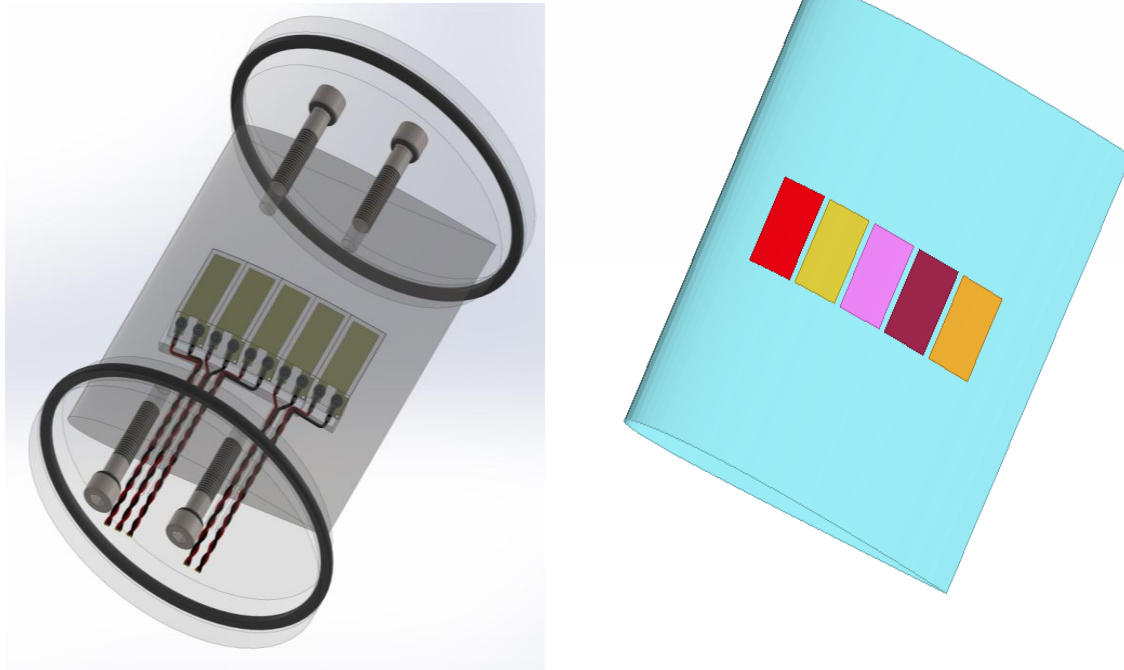


Figure 6.5: Variant of hydrofoil with PVDF films by experiment and by simulation

6.3 Discretization of model:

Partial differential equations that govern fluid flow are not usually working to analytical solution. So it is necessary to split domain in smaller sub domains or elements. The governing equations are than discretized and solved each of those sub domains. Continuity of solution across the common interface of two sub mains must be proper. Sub domain is categorized by different shape. The results can be influenced by the number of sub domains.

The discretization of the subdomain was realized using ANSA CAE. The hexahedral elements were used for the discretization. The domain has total 500129 hexahedron elements. The mesh density is higher close to the profile surface to obtain higher resolution within the boundary layer. The domain discretization close to the blade surface is shown in Figure 6.6.

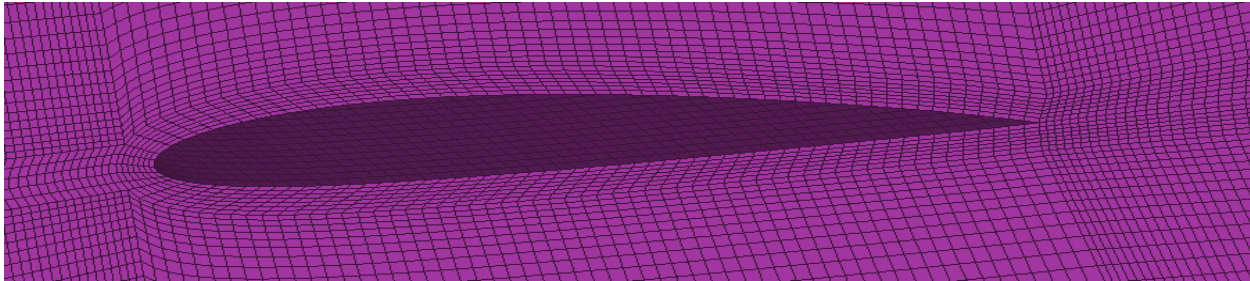


Figure 6.6: Detailed Mesh

6.4 Initial and Boundary condition:

Here, liquid domain has inlet and outlet section in opposite side. Liquid domain is covered by the walls from 4 different sides. As per experiment, the flow rate is 295 lt/s, inlet static pressure is 245 kPa, outlet static pressure is 125 kPa and ambient pressure is 100 kPa. Test section area at inlet is 150×150 m². Based on the volumetric flow rate and cross-section area, the velocity can be calculated from the relation below

$$Q = A \cdot V$$

$$V = \frac{295 \times 0.001}{0.150^2}$$

$$V = 13 \text{ m/s}$$

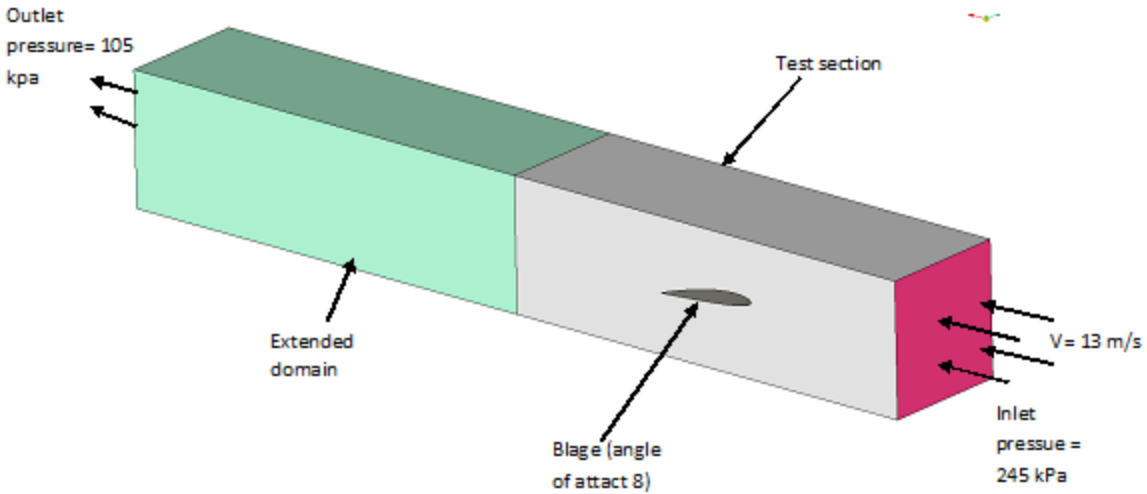


Figure 6.7: boundary condition on Test section

Fluent software is used for CFD analysis. The boundary conditions are 13m/s velocity at inlet, 245 kPa Inlet static pressure (Reynolds number= $Re = 1.57$, cavitation number = 1.71), 105 kPa static pressure at outlet and operating pressure is 0. At the beginning the whole domain is filled with water and the volume fraction of vapor is zero.

7. Testing of numerical models for cavitating flow simulations in selected regime.

7.1 Mixture modeling approach:

There are three models of multiphase approach as discussed before. All the models are applicable for considered problem. For the simulation the mixture model because it solves momentum equations for mixture and prescribes relative velocities to describe different phase.

7.2 Selection of cavitation model:

In CFD Fluent, three cavitation models are available. 1. Full cavitation model, 2. The Zwart-Gerber-Belamri model and 3. The Schnerr-Sauer model. The models properties were described before. Unlikely, full cavitation model led to computation divergence in case of partial cavitation.[5] In this case, the zwart-gerber-Balamri model is more preferable as it includes parameters which can be set according to the tested experiment. Cavitation properties are estimated as below according to experiment as follows

Vaporization Pressure $P_v = 3574\text{Pa}$

Bubble Diameter = $2\text{e-}06\text{ m}$

Nuclei-site volume fraction = $5\text{e-}05$

Evaporation co-efficient = 50

Condensation co-efficient = 0.01

Where, vaporization pressure is the minimum pressure for inception of cavitation bubble. Evaporation co-efficient is ratio of number of molecular transferred to vapor to number of molecules emitted from liquid phase and condensation co-efficient is ratio of number of molecules absorb by liquid phase to number of molecules impinging by liquid phase. [9]

7.3 Selection of turbulence model:

In section 4.4, Different turbulence models are discussed. The $k-\epsilon$ and the SAS-SST turbulence model can be used for unsteady sheet or cloud cavitation. The model employed in the present work is the shear-stress transport (SST) $k-\omega$ model. This model takes advantages of two worlds. In the viscous sub-layer region of a boundary layer, it uses a $k-\omega$ formulation and in the free stream, it switches to a $k-\epsilon$ behavior in the free-stream to cope with the free-stream turbulence properties. It is suitable for unsteady flow with adverse pressure gradients and separation.

7.4 Computation Approach:

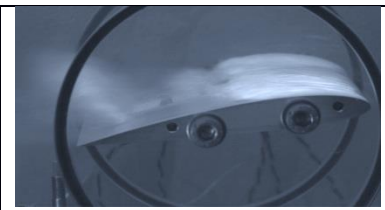
PISO method was used for the pressure velocity coupling. It gives faster convergence rate than SIMPLE method. PISO can maintain a stable calculation with a larger time step and an under-relaxation factor of 1.0 for both momentum and pressure. But it increased computation expenses if it is dealing with low time step but it is more accurate. Time step size for the simulation was 0.0005 second.

8. Comparison of the simulations with the experiments in the cavitation tunnel

In following sections, the data from experiment are compared with the CFD simulations. Measured PVDF signals are compared with the forces generated on the corresponding surfaces during the simulations. Camera records are analyzed and compared with the contours of volume fraction.

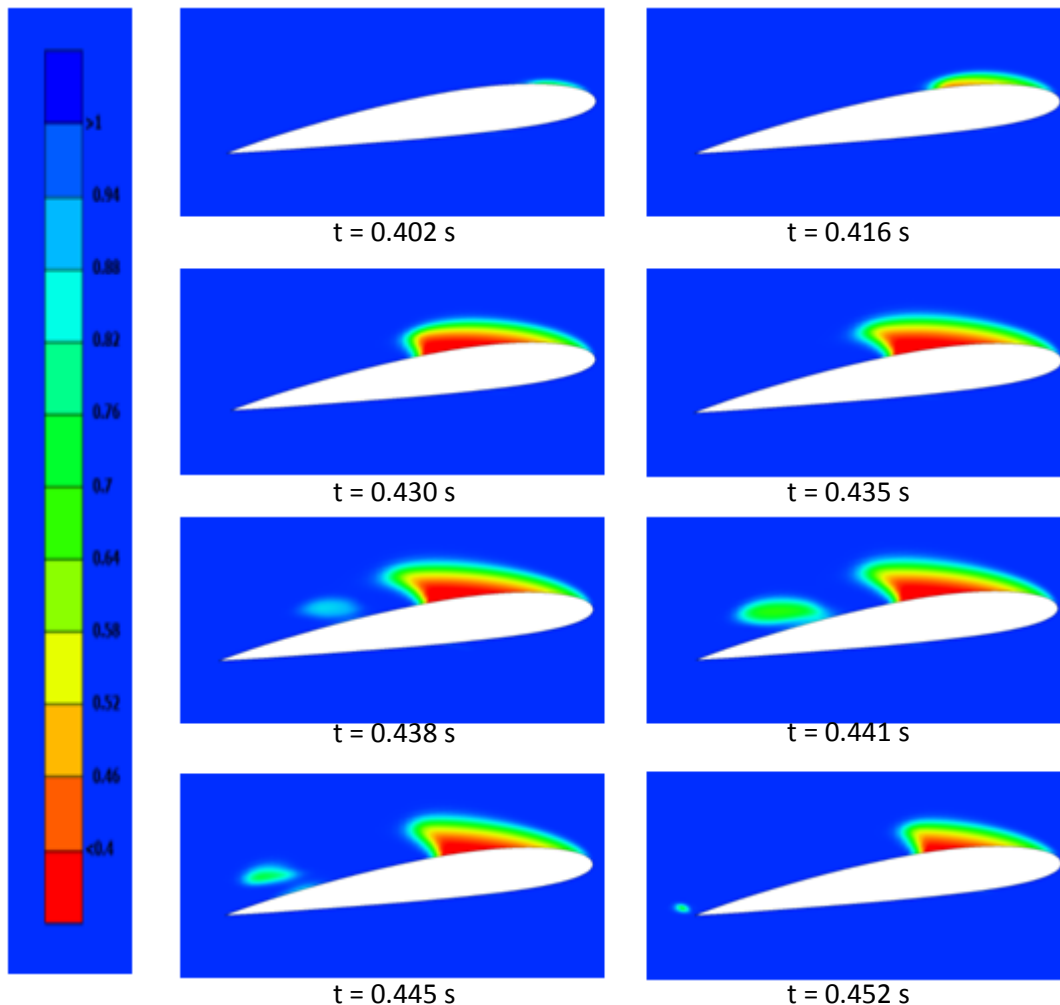
8.1 Mechanism of cavitation of Experiment:

Time	Image of test section	Description
T= 0ms		Inception of cavitation bubble does not produce on hydrofoil and this time, sheet cavity area is higher near to hydrofoil.
T=2ms		Inception of bubble cloud is just started and the mass transfer from water to vapor is in initial stage.
T=3ms		Bubble cloud size is increasing as shown in figure. It is moving from right to left in direction of flow. And sheet cavitation is decreasing which is moving from right to left.
T=4ms		Bubble cloud size is increased and at this time mass transfer from sheet cavity to bubble cloud is stopped. At that point, sheet cavity area is minimum.
T=7 ms		Bubble cloud size is increasing and moving from right to left. Sheet cavity area is increasing from its minimum area.
T=13 ms		Bubble cloud size reaches at its maximum size and that time pressure of cloud reaches at limit of vapor pressure. At that moment, sheet cavity area reaches at maximum level.

T=15ms		Bubble cloud collapse due to its pressure passed over limit of vapor pressure of bubble. It placed at trailing edge of Hydrofoil and from Figure it is shown at sheet cavity area is reached nearer maximum level.
T=16ms		Again inception of bubbles cloud takes place and at that moment, Sheet cavity area is still at maximum level. At conclusion, time period is 16 ms to finish one cycle of cavitation.

8.2 Mechanism of cavitation by Simulation:

The mechanism of cavitation is recorded from 0.4 second to 0.452 second. The images describe mechanism of cavitation to understand phenomena of cavitation and effect of bubble collapses.



8.1 Mechanism of cavitation by simulation

Mechanism of cavitation is shown in figure 8.1. In 1st image, sheet cavitation occurs near to the leading edge of blade at $t = 0.402$. Sheet cavitation covers 1st PVDF film at 0.416 seconds and sheet cavitation is increasing till 0.435 second, where cavity of bubble shedding over surface of 1st and 2nd PVDF and partially of 3rd PVDF, which shown in 4th figure. In 5th image, inception of bubble cavitation occurs near to 3rd PVDF film. Cloud shedding is moving in direction of fluid and it is shedding over 4rd PVDF film. 6th Image shows that cloud of bubbles increases which passes near to 4th PVDF film. Bubble can increase diameter till in reach limit pressure to its vapor pressure and in 7th figure, cloud of bubbles has maximum diameter at $t = 0.445$ s. The collapse occurs and due to that pressure or impact force occurs on Blade at $t = 0.452$ s and again sheet cavitation is started at leading edge and cavitation is also shown at tip in 8th Image. From figure 8.1, time period is 50 sec to finish one cycle of cavitation.

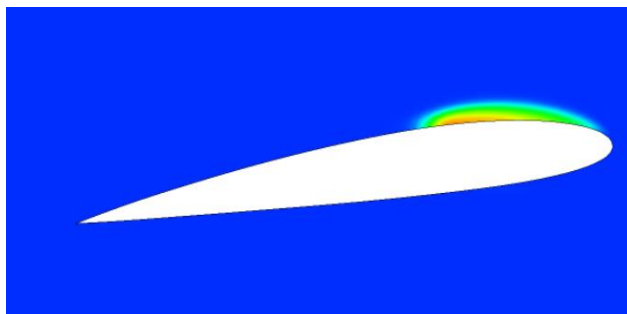
8.3 Comparison of the simulations with experiments by Visualization:

Comparison of mechanism of cavitation by simulations and experiments are divided in sub-process. The analysis is described below.

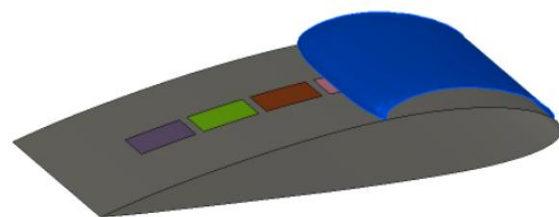
8.3.1 Inception of cavitations:



By experiment



By Simulation



Iso-surface

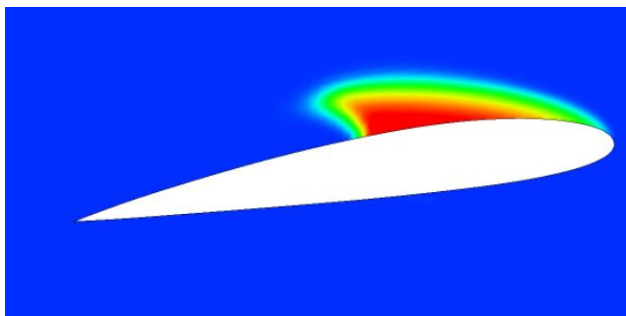
Figure 8.2 Comparison of inception cavitation by experiment and by Simulation

Inception of cavitation means pressure near to suction side of blade is reducing to its vapor pressure and due to that first bubble is produced in fluid. In figure 8.2, Inception of cavitation is shown by experiment and by simulation. Structure of cavitating flow occurs on the suction side of hydrofoil, which is shown in figure of iso-surface of blade.

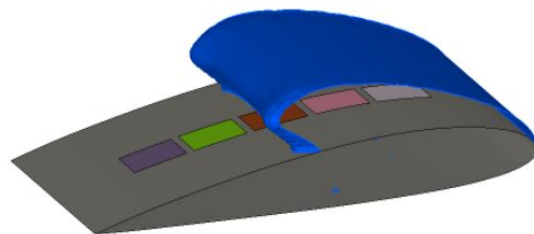
8.3.2 Sheet cavitation:



By Experiment



By Simulation



Iso-Surface

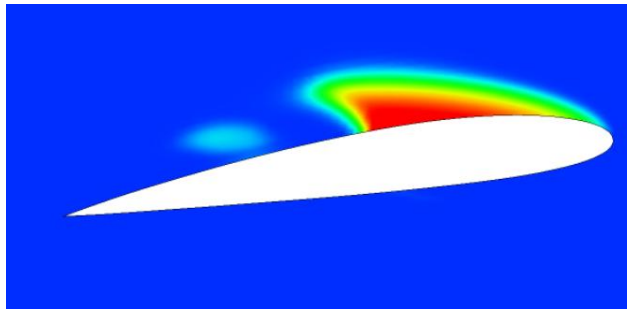
Figure 8.3 Comparison of sheet cavitation by experiment and by Simulation

Structure of cavitating flow by experiment and by simulation is shown in figure 8.3. A region of separated flow fills with vapor is shown in figure, which term as sheet cavitation. It covers suction side of hydrofoil and it covers first three PVDF film which seen in all three figures.

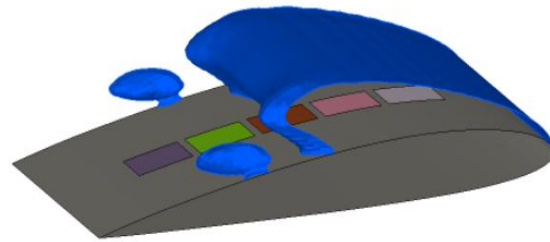
8.3.3 Inception of Cloud Cavitation:



By Experiment



By Simulation



Iso-Surface

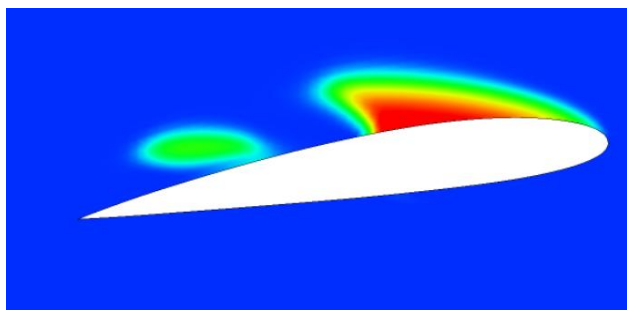
Figure 8.4 Comparison of inception of cloud cavitation by experiment and by Simulation

When the pressure of water near to surface is decreasing than its vapor pressure, the mass does transform from sheet cavitation into the bubbles cloud, which term as cloud cavitation. Figure 8.4 shows inception of cloud cavitation where cloud of bubbles is lifted from the surface of the hydrofoil. Inception of bubble cavitation is shown by figure by experiment and by simulation. Transformation from sheet cavitation to bubble clouds occurs near to 4th PVDF film which is shown in Isosurface figure 8.4. Formation of bubble cavitation is still in initial stage.

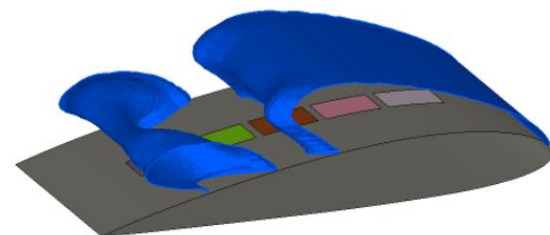
8.3.4 Cloud cavitation:



By Experiment



By Simulation



Iso-Surface

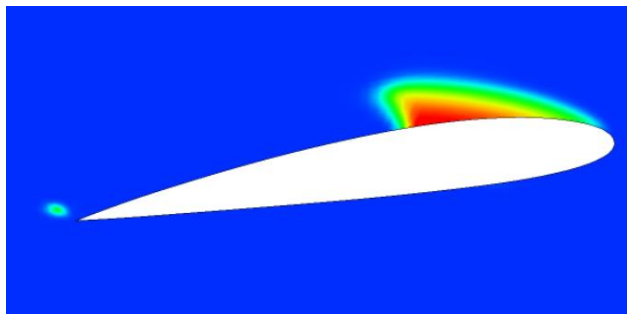
Figure 8.5 Comparison of cloud cavitation by experiment and by Simulation

The figure 8.5 shows that cloud of bubble is separated from surface of hydrofoil and it flows with water from right to left direction. At the same time, cavitating bubbles try to reach to its vapor pressure and it gains maximum size (diameter) which shows in figure 8.5 simulations. The cloud bubble is nearly at the same place which shown by experiment and by simulation.

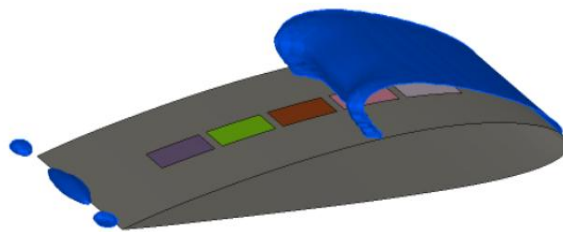
8.3.5 Collapse of Cloud Cavitation:



By Experiment



By Simulation



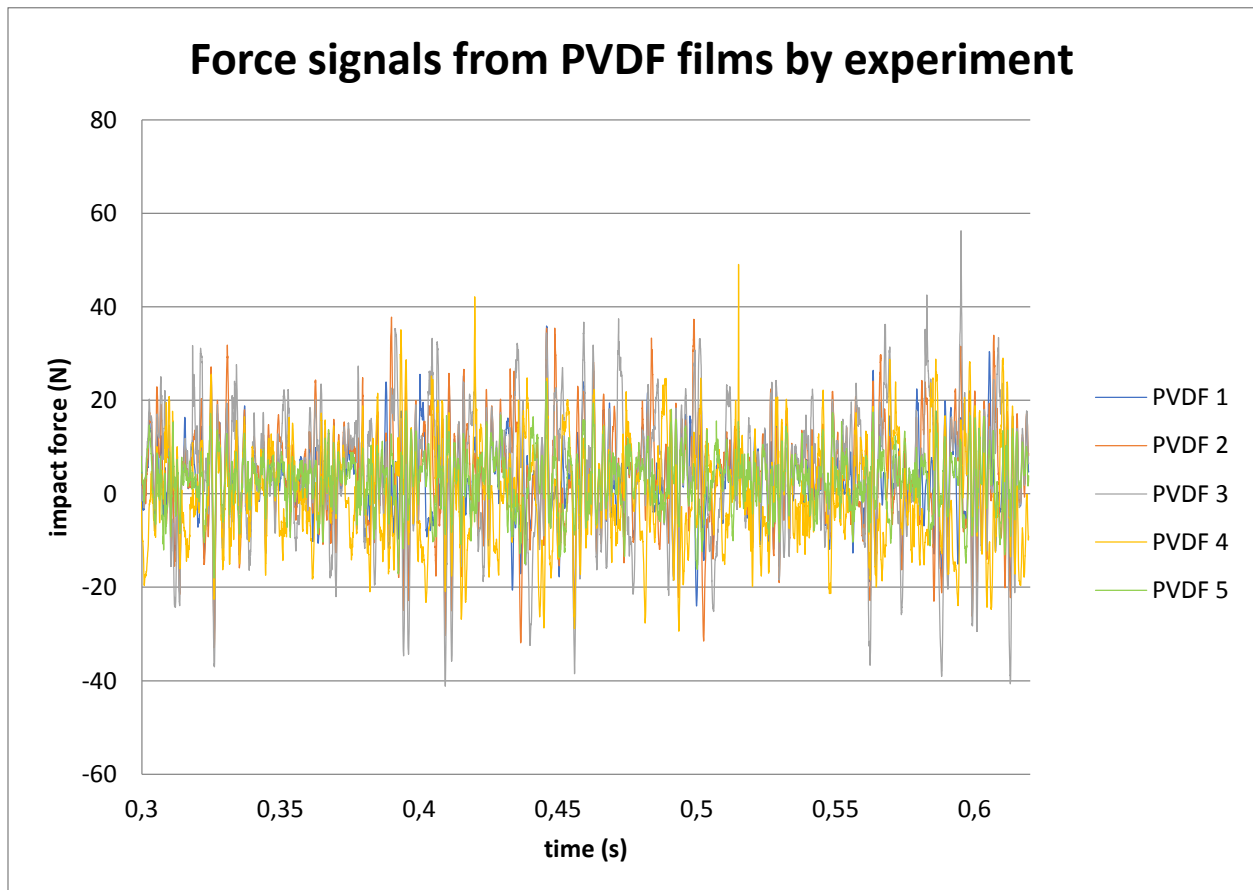
Iso-Surface

Figure 8.6 Comparison of collapse of cloud cavitation by experiment and by Simulation

This is last process of the cavitation mechanism. Here, bubble itself trying to increase pressure as increase diameter till its limiting pressure (vapor pressure). When it overcomes limit of pressure (vapor pressure), bubble cloud is collapsing and due to collapse, it produces shock wave near to surface of hydrofoil. And it damages the tip of hydrofoil. This effect is clearly seen in figure 8.6.

8.4 Comparison of Simulations and experiments by PVDF films:

In Simulation, 5 different areas are used on blade, which are exactly same place of 5 PVDF film as use in experiment as shown in figure 6.5. Comparison signals of PVDF films by experiments and signals of PVDF films by simulation are given as below. Important note is that, voltage distribution respect to time is being measured in experiment and signals were calibrated for measuring impact force by using a drop ball test method. And Impact forces distribution are measured with respect to time by simulation.



8.7 Force signals from PVDF films by experiment

The impact force is measured by different PVDF films in experiment, which can be shown in figure 8.7. By this figure, force varies from -40 N to 60 N from 0.3 to 0.62 second. Strong impact forces are measured by 3rd and 4th PVDF film. In this time period, PVDF 3 and PVDF 4 have more damage due to bubble collapses or by cavitating flow. In this time period, PVDF 1 and 5 have lower damage compare to other PVDF films.

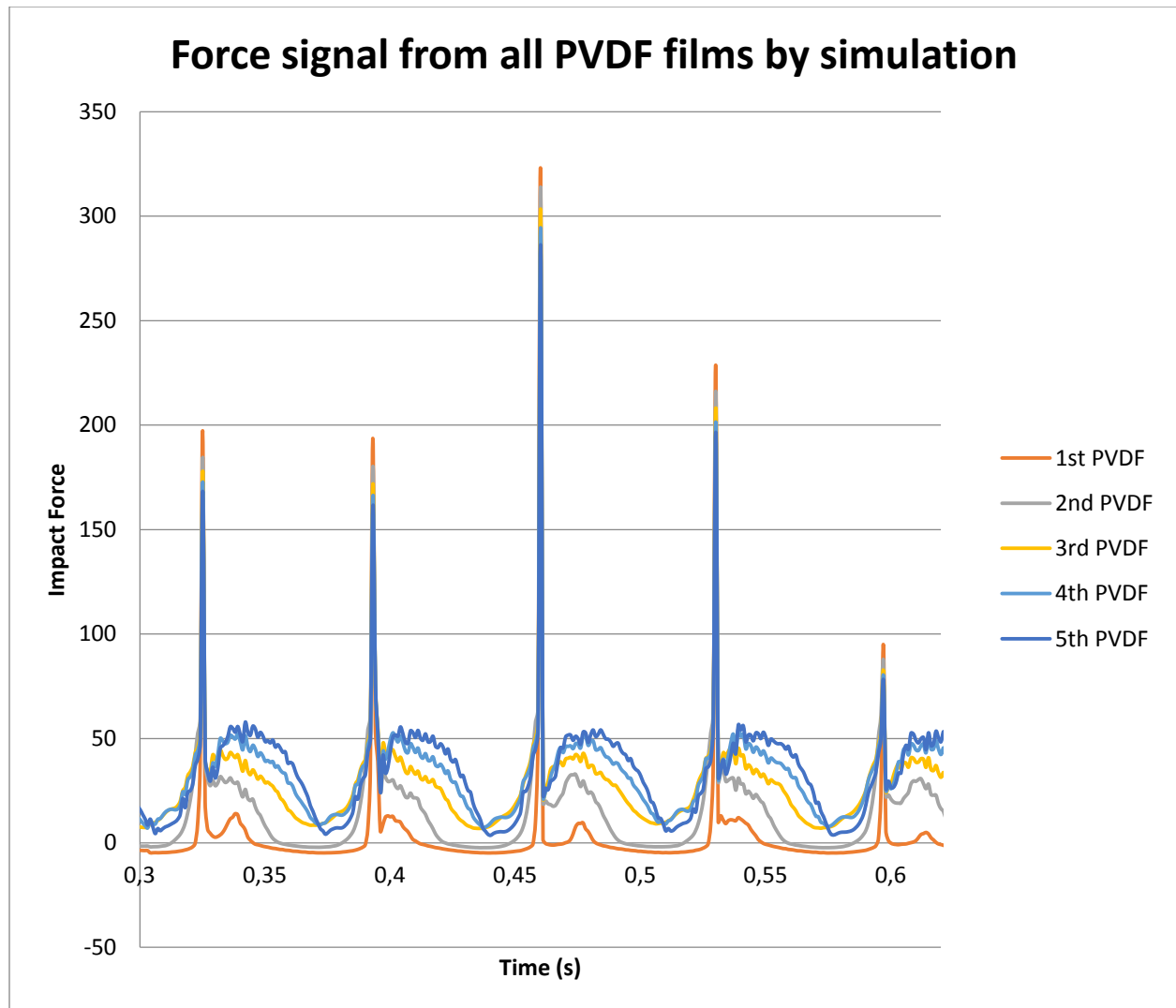


Figure 8.8: Force signal from all PVDF films by simulation

In figure 8.8, Force signal are calculated on surface on PVDF films from 0.3 s to 0.62 s time by simulation. Here impact forces are fluctuating between 0 to 50N by cavitating flow. Due to collapse of bubble, impact value of force is between 150 N to 330 N by simulation. Due to cavitating flow, PVDF film 4 and PVDF film 5 have more damage because higher impact value of force is 50 N. Due to collapse of cloud bubble, whole hydrofoil has higher impact load from 200 to 330 N.

8.6 Comparison of Simulations and experiments by Hydrophone:

Hydrophone is more accurate compare to the PVDF film in term of sensitivity of impact force and it placed near to the tip of Hydrofoil. It is used to measure Erosion damage on tip by bubble collapses.

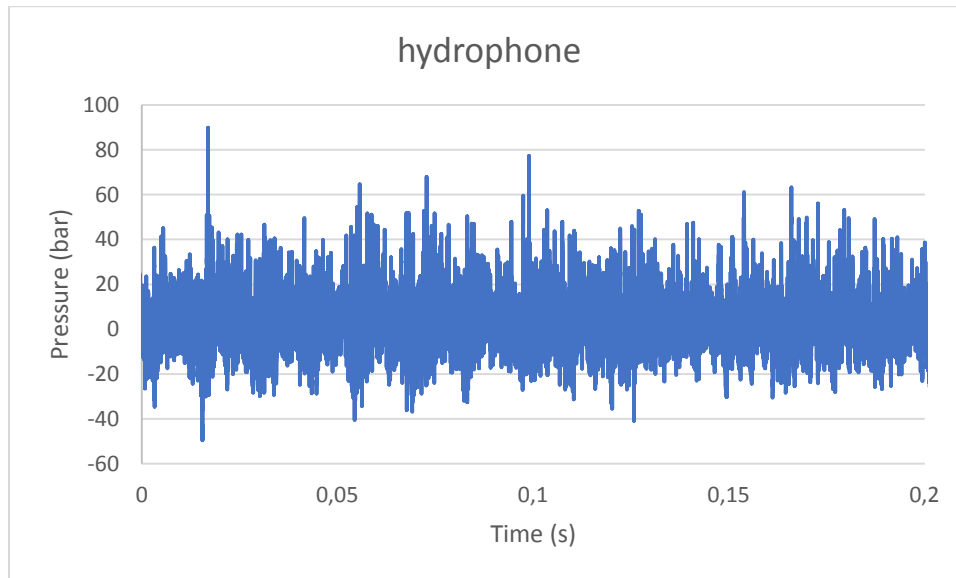


Figure 8.9: Pressure signal from hydrophone:

In figure 8.9, the measurement is given from 0.1 to 0.2 second. It shows peak pressure is at 90bar, when the impact of collapse of bubble is higher. This figure shows pressure fluctuation is in between -50 to 100 Bar on hydrophone. The cavitating flow is very aggressive near to tip of the blade. By simulation of hydrophone result is not so accurate because Pressure at one point is difficult to analysis with respect to time by FLUENT software. The model is divided in very small elements by finite volume analysis method, so point load is not defined in discretized model.

8.6 Comparison of PVDF signal and Photos of Experiment:

Specific low time period is required to understand force distribution for specific time. It helps to compare between visualization from camera and signal from PVDF which describe as below. Time period is taken for comparison from 0.55 second to 0.6 seconds in experiment.

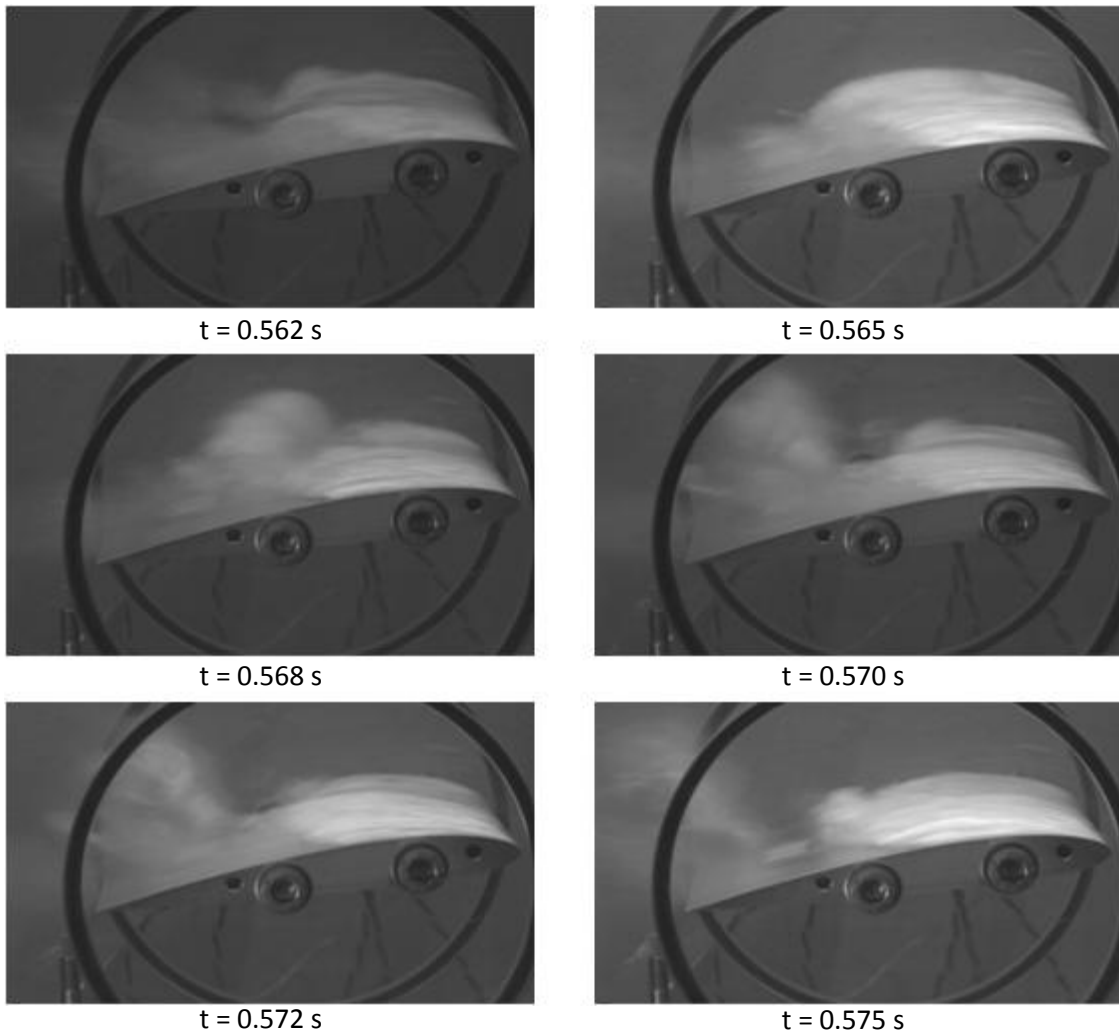
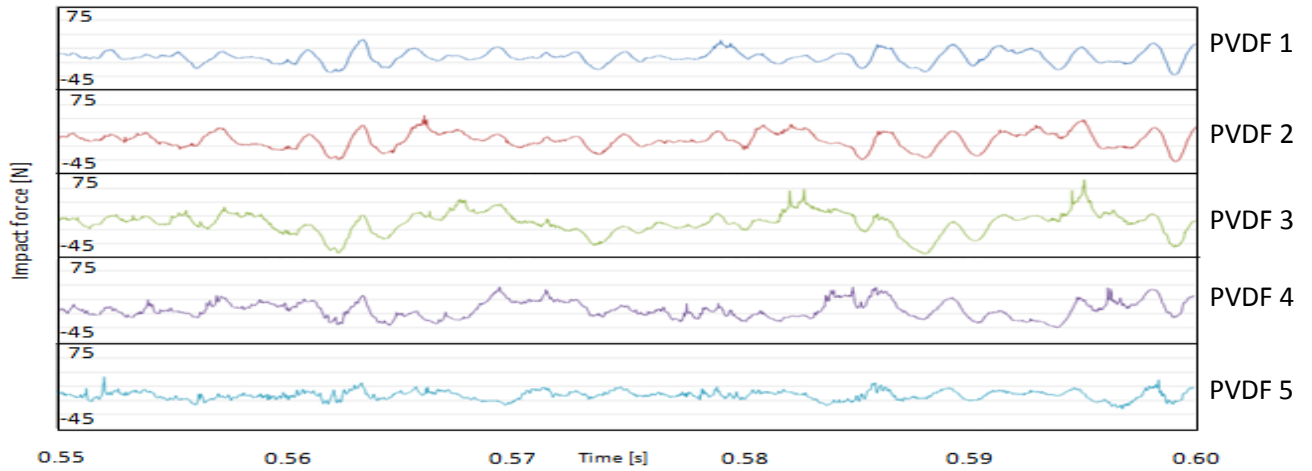


Figure 8.10: comparison of signal from PVDF film and images of experiment

As shown in figure 8.10, 1st Image of experiment shows that inception of cavitation occurs at 0.562 second. Impact load is higher on first PVDF film which is about 40N at that time as is shown in figure. Cavitation occurs on the top of first PVDF film. So Impact force applied on first PVDF film is higher at 0.562 second compare to another PVDF films as from signal figure.

2nd Image of experiment shows that sheet cavitation occurs at leading edge of hydrofoil. 1st, 2nd and 3rd PVDF films are covered by sheet cavitation at time 0.565 s. Here 4th PVDF film is partially affected by cavitation. From signal result, impact forces are higher on 1st and 2nd PVDF film (Leading edge of hydrofoil) than 3rd PVDF and 4th PVDF films respectively. Highest value of Impact force is on 2nd PVDF around 30 N, and lowest value of impact force is 2N on 1st PVDF film.

3rd image of experiment shows that inception of cloud cavitation is produced at time 0.568 second between PVDF film 3rd and 4th. So, Impact forces on 3rd and 4th PVDF film are higher compare to other PVDF films. From Signal data, impact force on 3rd and 4th PVDF films are 36 and 37 N respectively, which are higher than other PVDF films in figure of signals.

4th Image of experiment shows that cloud bubbles are shedding on PVDF 4 and PVDF 5 at $t = 0.441$ s. Effect of impact force on 4th PVDF film is higher than effect of forces on other PVDF films and from shown in signal figure, impact force value at PVDF 4 is 36 N. from signal figure, impact force value on 5th PVDF film is zero. Cloud bubble does not effect on 5th PVDF film so this bubble is week bubble intern of energy.

5th image shows that cloud cavitation is shedding on 5th PVDF film (near to trailing edge) at $t = 0.572$ s. Cloud bubble impacts on 5th PVDF film and its value is 20 N which shown in signal figure. At the same time, sheet cavitation covers first two PVDF films, so impact force values of sheet cavitation are around 5 N on theses PVDF films.

6th PVDF film shows that cloud bubble already passes the hydrofoil at $t = 0.695$ s. so, there is not strong impact force due to any collapses or by sheet cavitation on hydrofoil, which can be seen by figure signal. In 6th Image, sheet cavitation covers first 3 PVDF films but sheet cavitation is not so aggressive to convert in vortexes, so Impact force on leading edge is not too high at $t = 0.573$ s.

8.7 Comparison between Simulation Images and Signal of force:

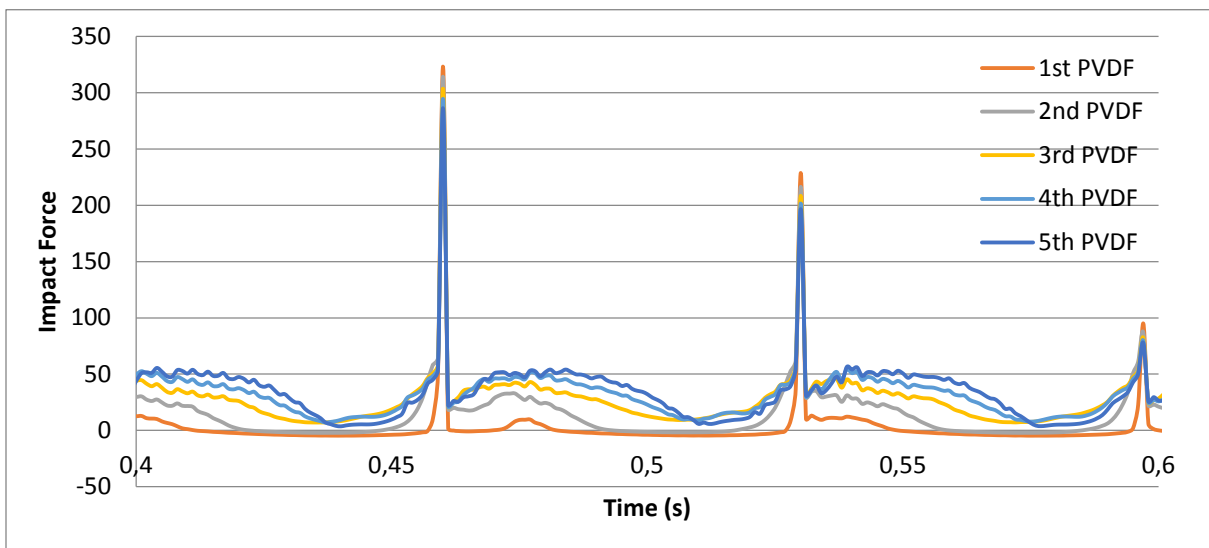
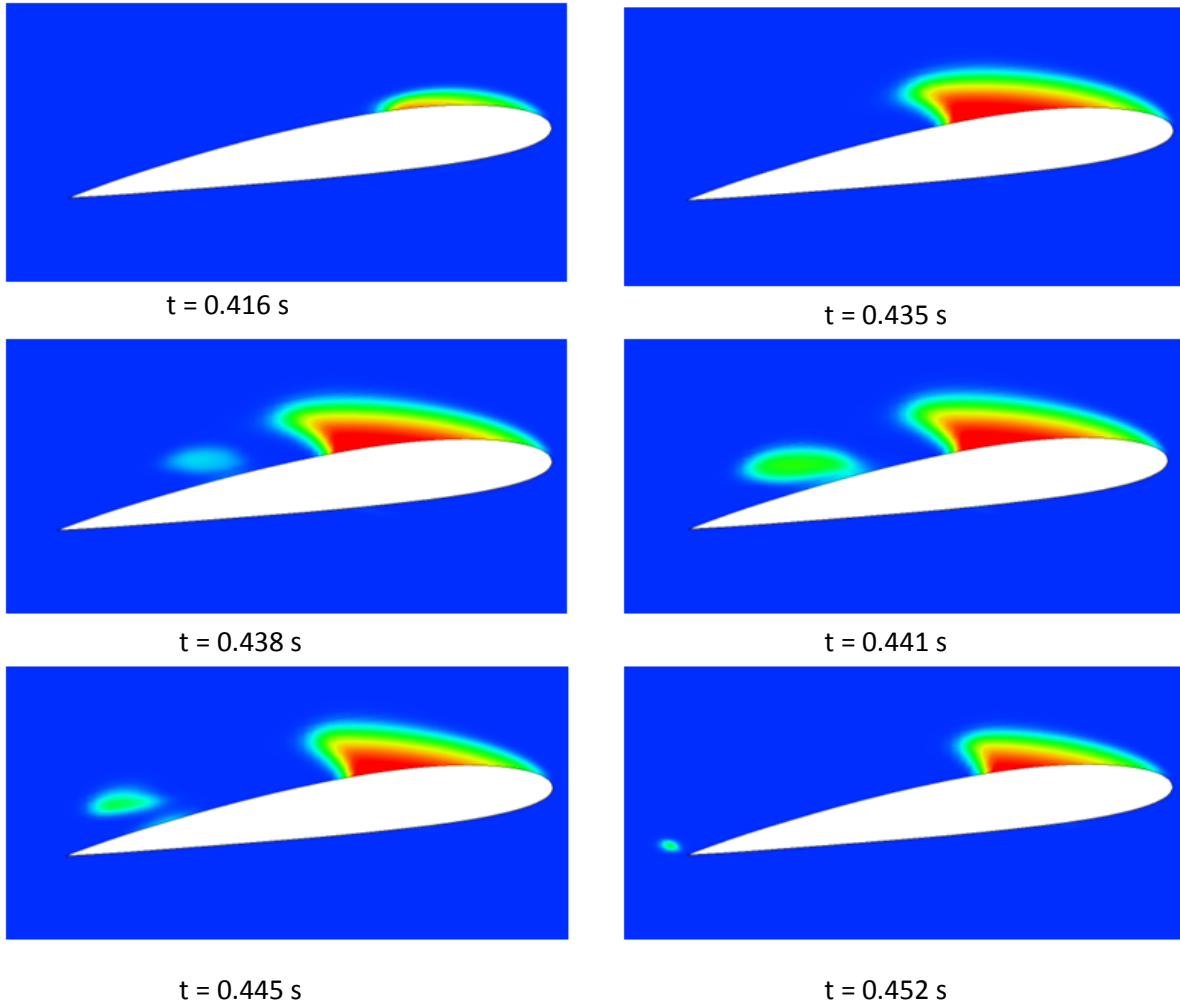


Figure 8.11 comparison of image and signal of impact force for each PVDF films

First image shows of simulation that, inception of cavitation occurs near to first PVDF film at 0.416 second and impact force is zero because no collapses occurs at that point and no vortex generated in flow. But there still effect of on other PVDF films by previous collapse of bubbles. Impact force due to previous collapse are 50, 45, 31, 15 N on 5th PVDF, 4th PVDF, 3rd PVDF and 2nd PVDF respectively. Impact of previous bubble collapse is decreasing with time as shown in 8.11 figure of signals.

Second figure of simulation shows that sheet cavitation occurs and it covers 1st and 2nd PVDF film at 0.438 s. The impact force due to sheet cavitation is negligible as shown in figure signal. The impact forces on trailing edge are decreasing with respect to time.

Third image shows that inception of cloud cavitation occurs at $t = 0.438$ second on surface of 3rd PVDF film. Due to that impact force on 3rd PVDF film is around 10 N. Impact force on 4th PVDF and 5th PVDF films are 5 and 4 N respectively. Effect of cloud cavitation is shown on 4th and 5th PVDF by figure of signals.

Fourth Image shows that travelling of cloud of bubbles on 4th PVDF film at $t = 0.441$ s. so, Impact force on 4th PVDF film is around 10N as shown in figure of signals.

Fifth Image of simulation shows that cloud cavity is shedding over surface of 5th PVDF film at 0.445 s. Due to impact of cloud cavity, impact force on 5th PVDF film is 25N and sixth image shows that cloud of Bubble collapses at tip of Hydrofoil. Impact of collapses effect on surface of all PVDF films which is shown in figure of impact force signals. Value of Impact force is between 300 to 330N on surface of PVDF films.

8.6 Interested regimes:

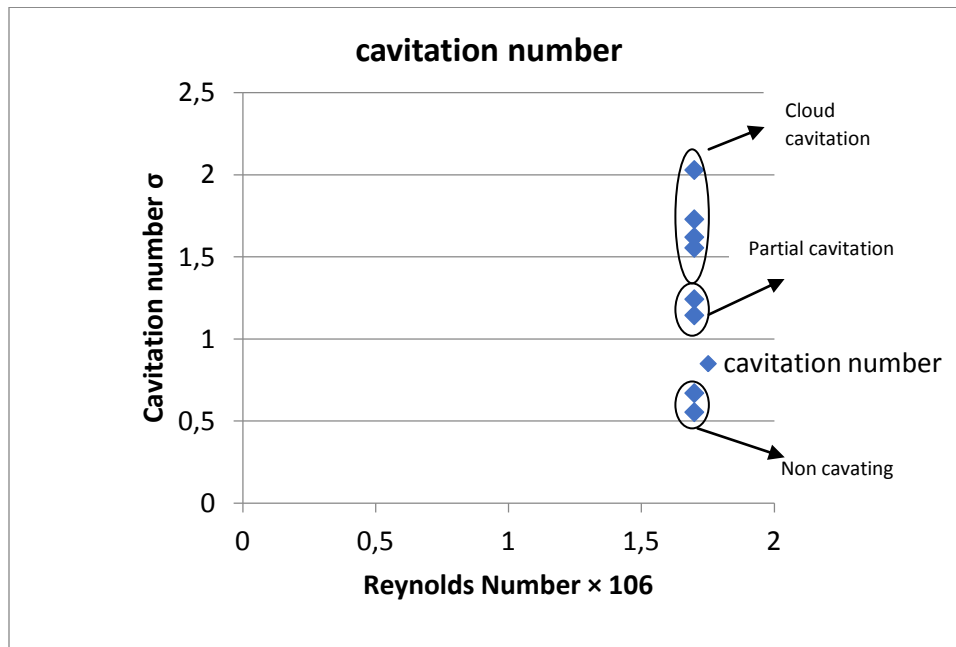


Figure 8.12: relationship between Reynolds number and cavitation number

Figure 8.12 shows the combination of cavitation number and Reynolds number used in simulations. These regimes range are between cavitation number $\sigma = 0.55$ to 2.03, where Reynolds number is 1.71×10^6 (295 lt/min) and inlet pressure is 245 kPa and range of outlet pressure is between 70 to 145 kPa. The figure shows that, cloud cavitation is increasing with increasing cavitation number at same Reynolds number and maximum limit of cavitation number is 2.03. At lower value of cavitation number from 0.5 to 0.8, no cavitation occurs in test-section.

9 Comparison of frequency analysis by Simulation and by Experiment:

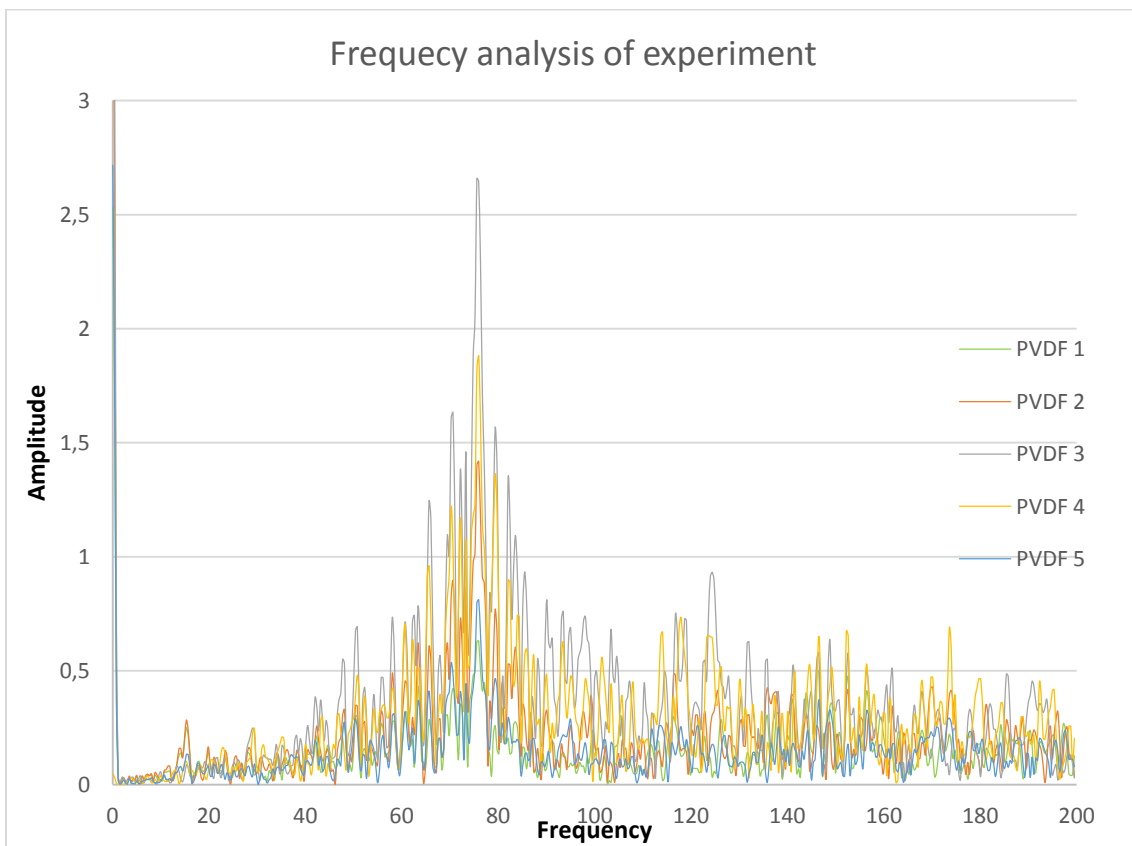
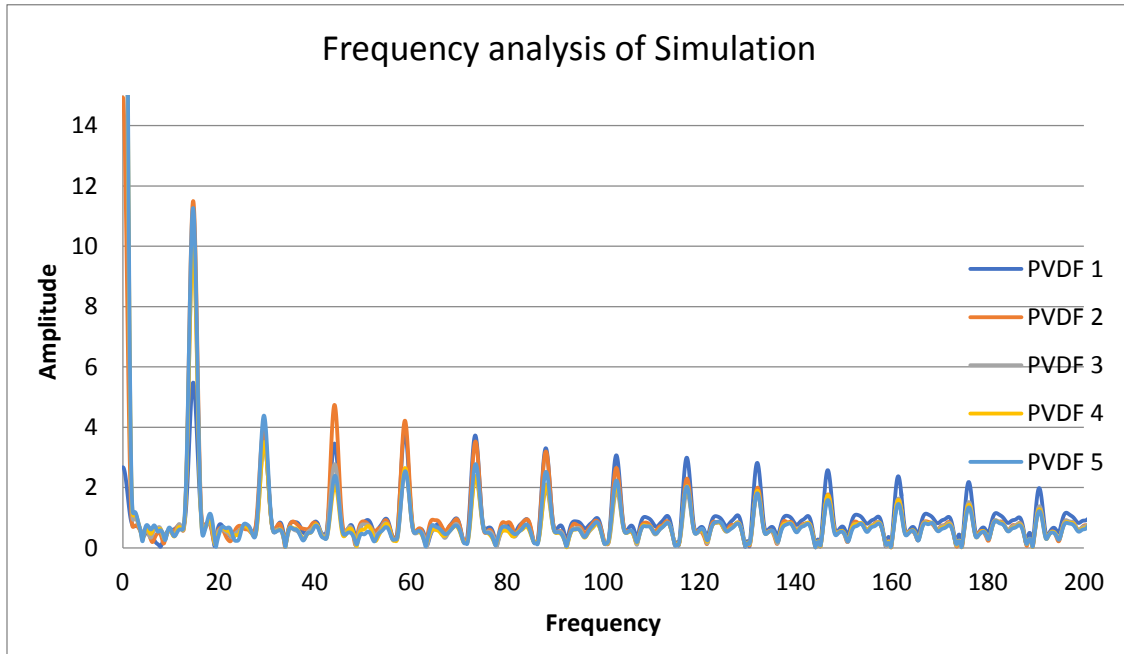


Figure 9 Comparison of frequency analysis of Experiment and of simulation

Comparison of frequencies from simulation and from experiment is shown in above figure 9. By analyzing data from experiment, cavitating flow has higher amplitude of 78 Hz on 3rd PVDF film compare to other PVDF films. It means impact of cavitating flow is higher on third PVDF film. The frequency range is 200 Hz where peak value of amplitude is 3 at frequency 78 Hz. It means time collapses of bubble is 14 ms which has amplitude value is 3.

By analyzing data from simulation, 2nd PVDF is affected by higher amplitude of cavitation around 11 at 16 Hz frequency. By this result, 2d PVDF film has higher impact of cavitation compare to other PVDF films. And time period of collapse is 62ms.

By comparing the frequency analyses of simulation and experiment, the results are quite similar at frequency around 75 Hz and amplitude values are quite similar, which is around 3 to 4. But amplitude of impact force is Maximum at low frequency which is around 16 Hz by simulation, when amplitude value of impact force is quite low at low frequency by experiment as shown in figure 9. At conclusion, sensor of PVDF film cannot be too precise or accurate at low frequency collapse or PVDF signal is not calibrated well enough to sense low frequency collapses.

10. Data Analysis of impact force by histogram:

10.1 Data Analysis for experiment:

The PVDF film sensors sense peak signal when bubble collapse occurs. The sampling frequency of signal is 100 KHz, the magnitude of peak is 150 N. here, and the magnitude of peak represents the measured individual impact load. Data is measured from each of five PVDF films sensors.

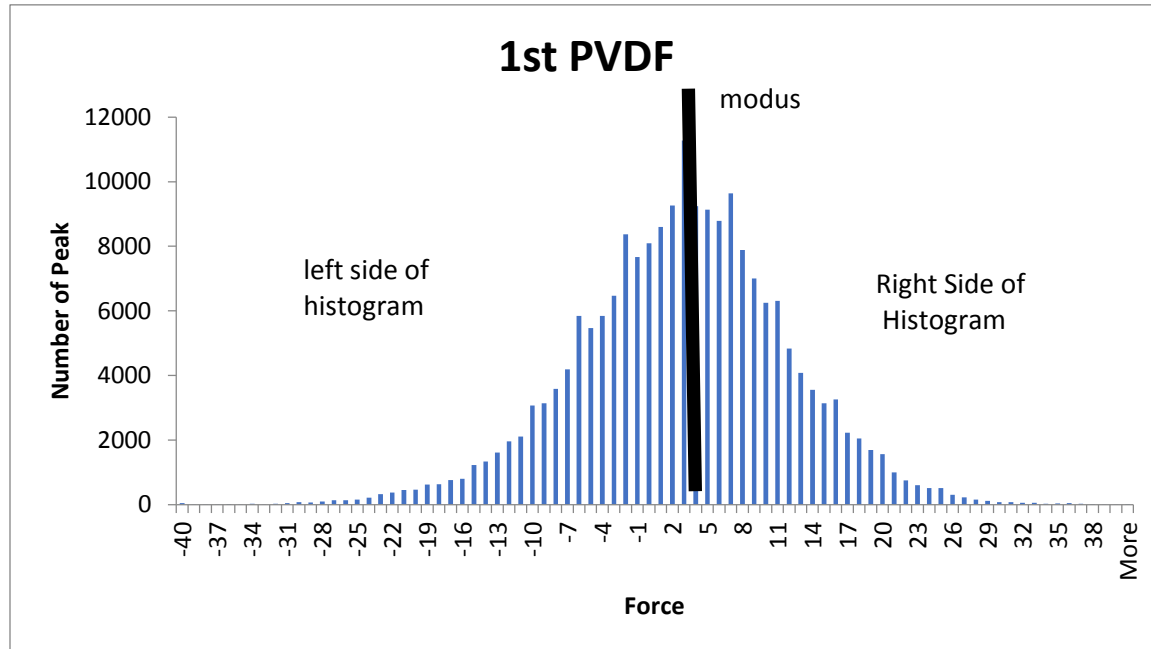


Figure 10.1 Histogram of Impact force detected by 1st PVDF film.

By the Signal, all data of positive and negative peaks are measured automatically. The signals are analyzed as shown in figure 10.1 for 1st PVDF film and other figures are shown in appendix (a). For Ideal situation, Distribution of the signal peaks is normal where negative and positive peaks values are same. But due to effect of bubble collapse, vibration occur which convert distribution of signals in disrupted form as shown in figure 10.1. The left and right side of histogram of peak count are divided by modus of force. We tried to figure out peak value of impact force related to bubble collapse in non-symmetry of distribution of signal.

Next step is to mirror the left side of histogram around modus to see the different caused by occurrence of collapses of bubbles which is shown in below figures for each PVDF films.

From figure 10.2, the right side (smooth) signal is considered in red color and left side signal considered in blue color. Both signals are coincident at one point as shown in figures which is considered as limit. When all positive signals are below than this limit, it is called as noise. And when all positive signals are higher than this limit, it is called as collapses of bubbles. This value is different with different PVDF film as its position.

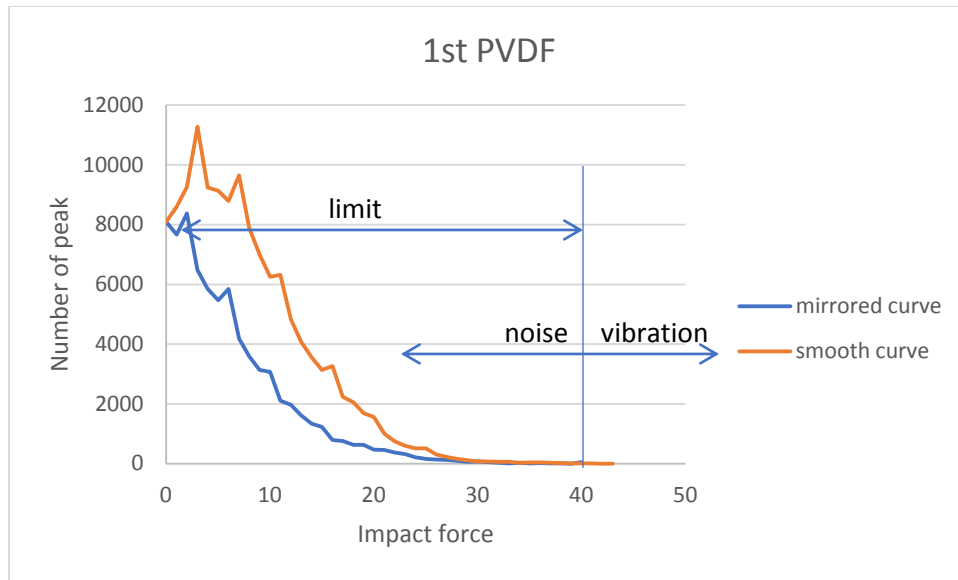


Figure 10.2 Modified Histogram of impact force at 1st PVDF film

Here as shown in figure 10.2, the limit impact force at 1st PVDF film is 40 N.

The higher value of limit is selected by comparing each PVDF sensor signals as shown in appendix (b). We consider that the limit is 55 N which is observed in each mirrored histogram result of PVDF films signals.

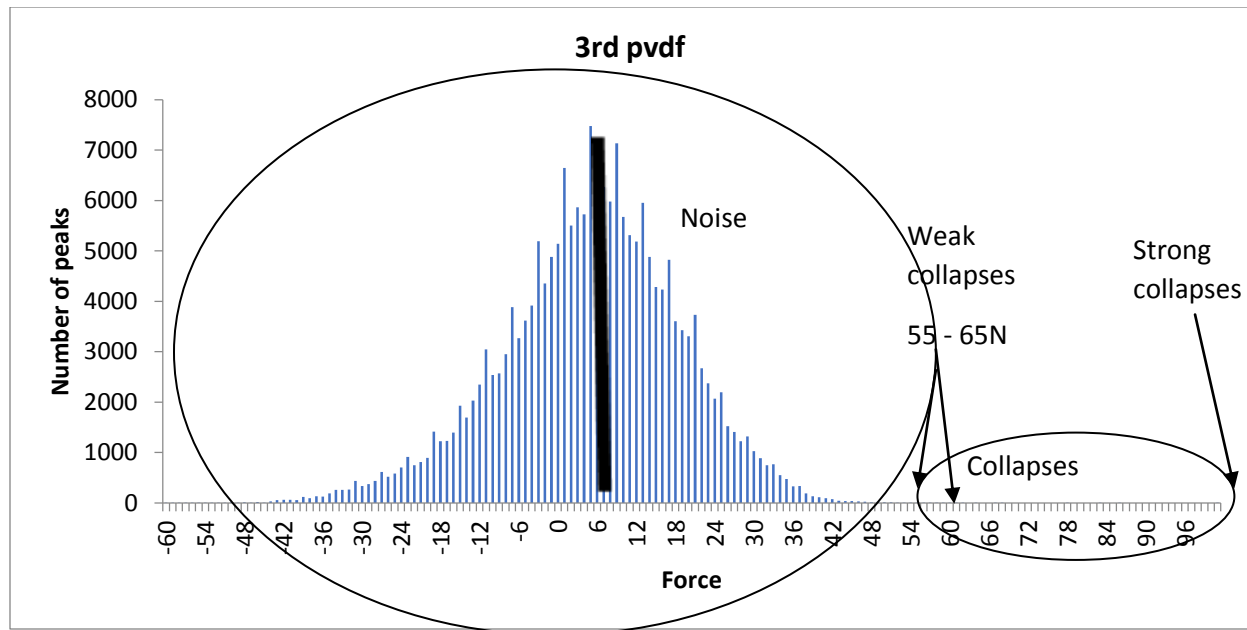
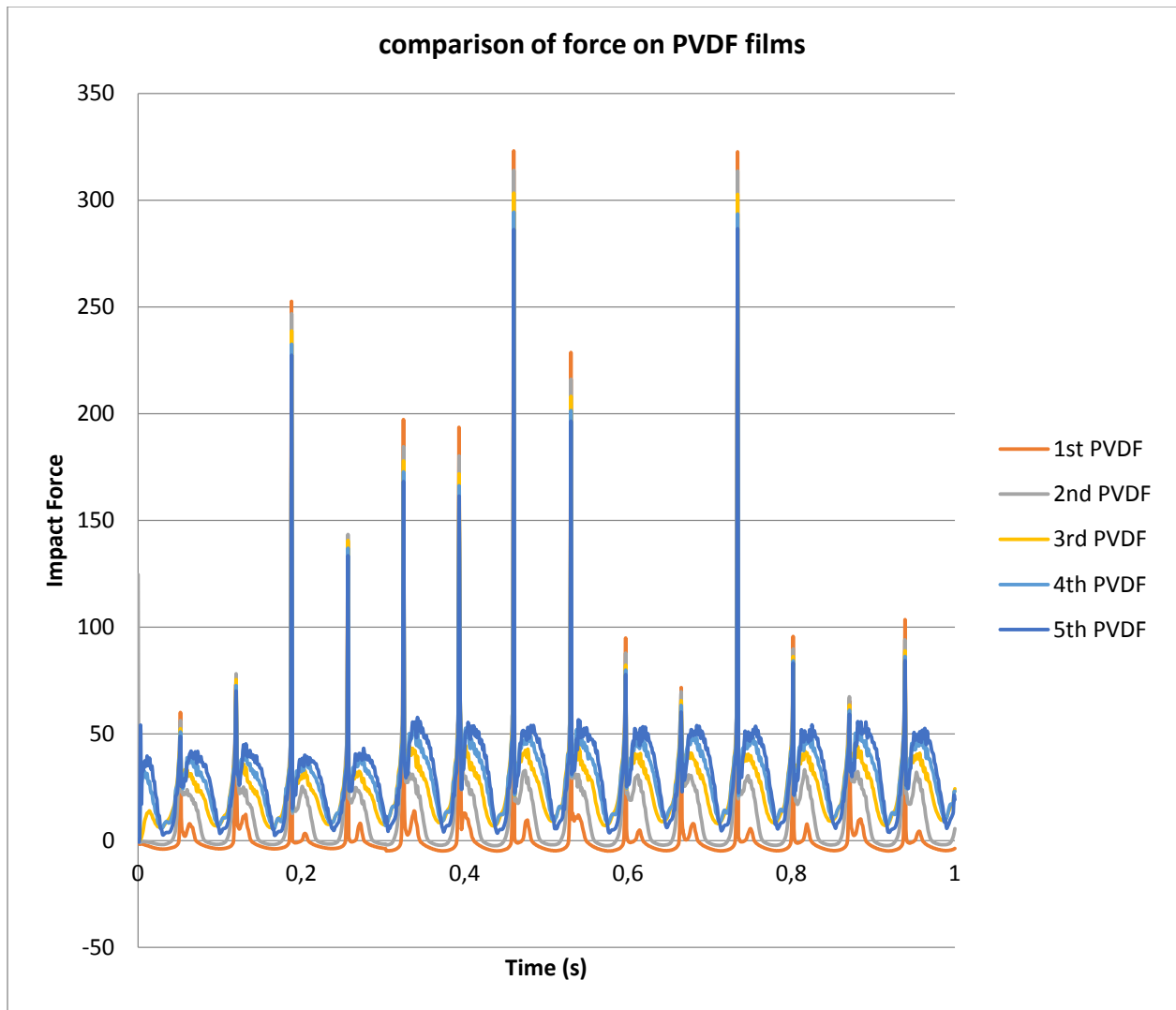


Figure 10.3 Analysis of Histogram of Force of 3rd PVDF film

Here, the result shows in distribution signal from 3rd PVDF for selected regime where $Re = 1.73 \times 10^6$, $\sigma = 1.73$ (290l/s, inlet pressure 245 KPa). As shown in figure 10.3, limit force is 55 N. The lower value than limit force is considered as noise and higher value of force than limit force called as Vibration/ Collapse. Weak collapses occur from 55 to 70 N and Strong value of collapse is 100 to 330N. Note that 55 N is higher limit from each PVDF film by comparing all modified histograms. So 55 N impact force as limit is considered for each PVDF films.

9.2 Data Analysis for Simulation:

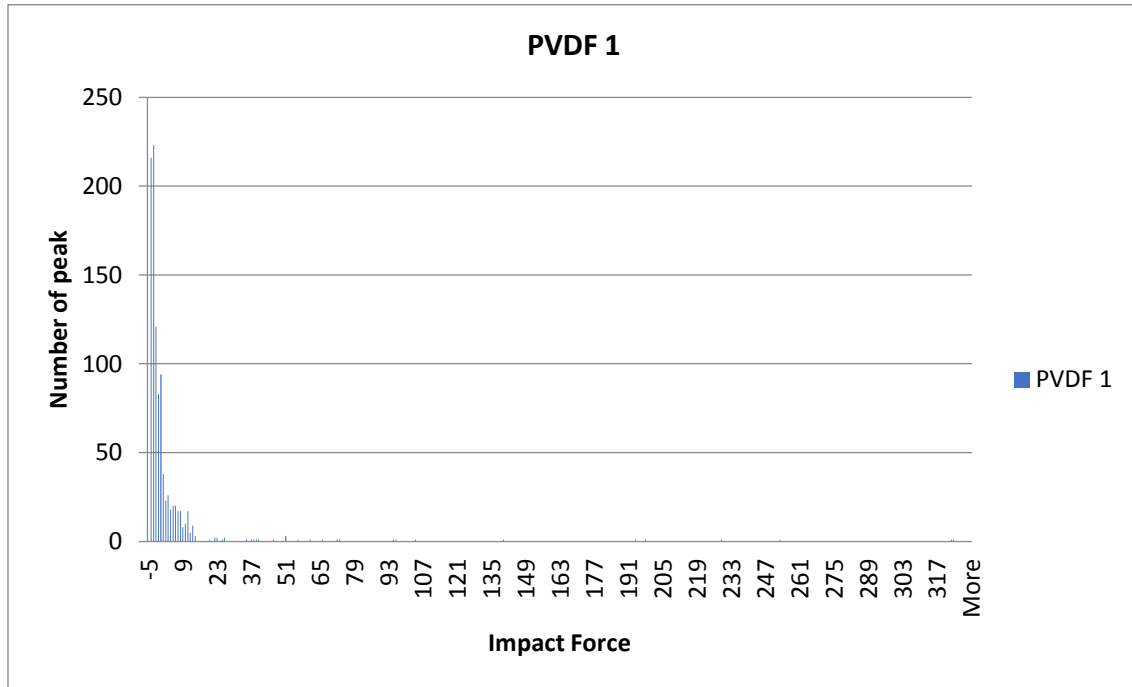
In Simulation model, 5 PVDF areas are defined on surface of the model which is shown in figure 6.5. The sampling frequency of signal is 1 KHz; the magnitude of peak is 325 N. Here, the magnitude of peak represents the measured individual impact load due to collapses. Data is calculated by monitoring force at each of five PVDF films in model in time period. Each data set is 1 second long.



10.4 Comparison of Impact forces on PVDF films by Simulation

As shown in figure 10.4, Impact force due to cavitating flow is increasing from PVDF 1 to PVDF 5. Near to PVDF film fluctuation in impact force is higher compare to other PVDF films. Due to collapses of cloud bubble, peak value of impact force at 1st PVDF film is higher around 320 N compare to 5th PVDF film by simulation.

10.2.1 Data analysis of Impact force:



10.5 Histogram of Impact force detected by 1st PVDF film

As discussed in last paragraph, the Impact force of cavitating flow is increasing from leading edge to trailing edge of Blade as in figure 10.4. But in Histogram of each PVDF films, Number of peak at different impact load is shown in figure 10.5 and in appendix (c), which help to understand or evaluate erosion potential at each point of PVDF film. In all figures of histogram of impact force which are in appendix (3), number of peak are highest at low impact force. Due to large number of peak at low impact force are producing noise. So as per experiment, 55 N is selected as limit impact force. Below that force is consider as noise which is not as harmful as values above impact forces, And above value of limit force is as considered as Vibration or collapses near to PVDF films.

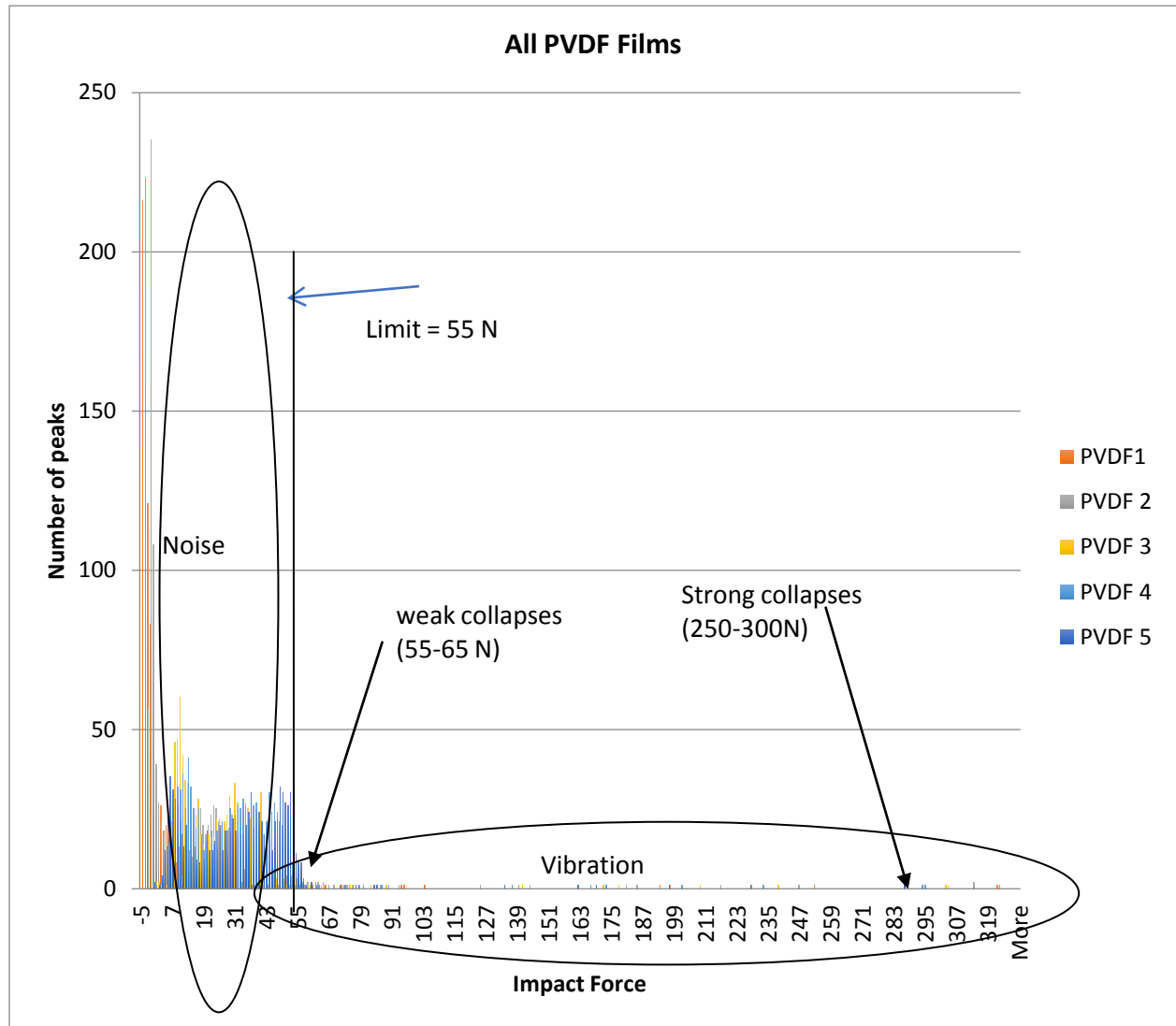


Figure 10.6 Analysis of Histogram of Force for all PVDF films

In figure 10.6, the limit force is considered as 55 N. due to limit force, noise is produced the load from 0 to 55 N on blade and Due to bubble collapses, the impact force of blade is between 55 to 330 N. Here, 55 to 65 N of impact load are considered as weak collapses on surface. Numbers of peaks are higher by weak collapses than impact force occurs because of strong collapses (250-330 N). At 5th PVDF film, the noise level is too high compare to other PVDF film as shown in figure 10.6.

10.3 Comparison of Histogram of cavitation collapses by Experiment and by Simulation:

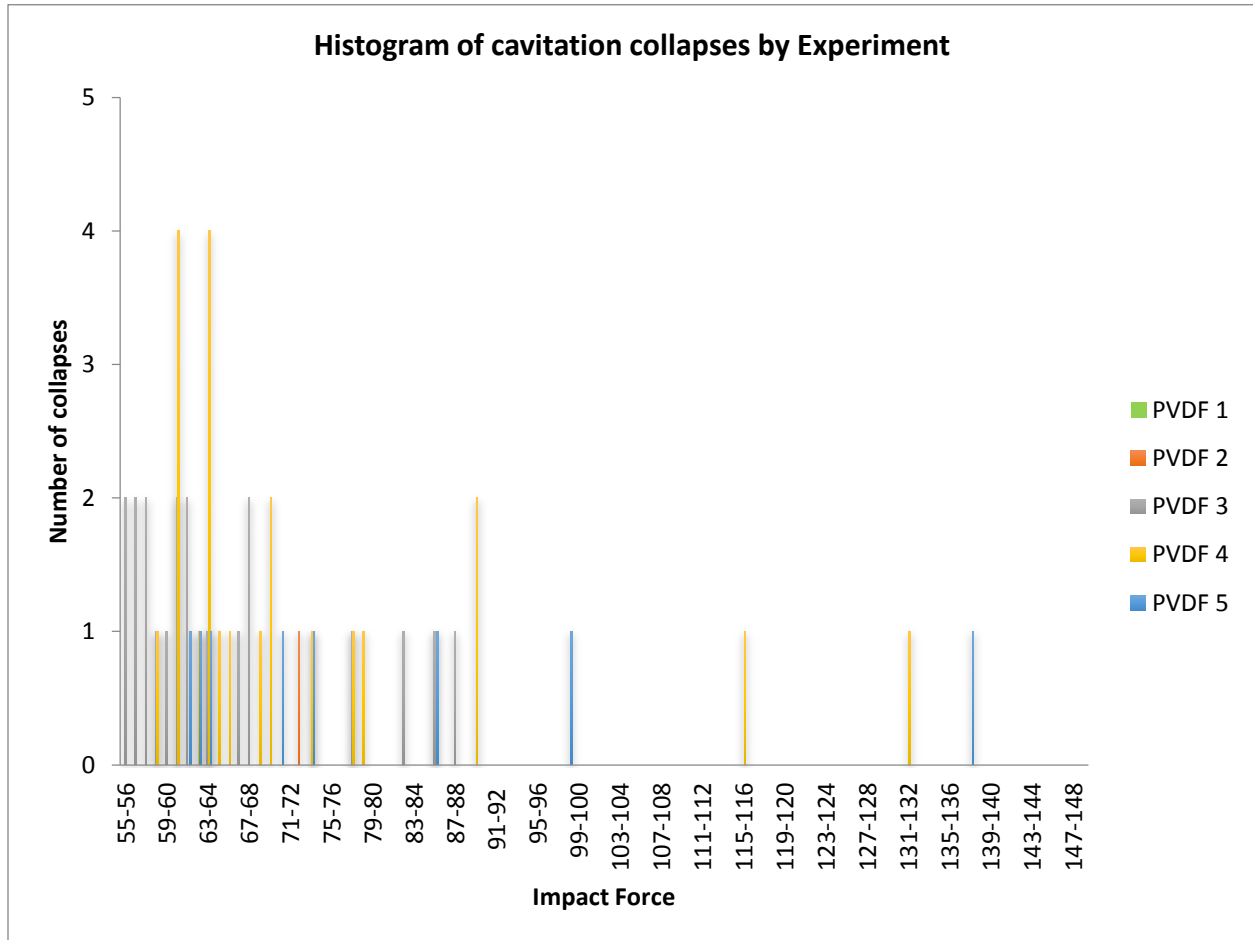


Figure 10.7 Histogram of cavitation collapses by experiment

An example of final results for specific regime when $Re = 1.73 \times 10^6$, $\sigma = 1.73$ (290l/s, inlet pressure 245 KPa) is shown in figure. The figure 10.7 shows a histogram of collapse which is detected by five different PVDF films at different position. From experiment and by signal, the strongest and highest numbers of collapse are detected by PVDF film nearest to trailing edge (PVDF 5). Only the weak collapses occur nearest to the leading edge of blade.

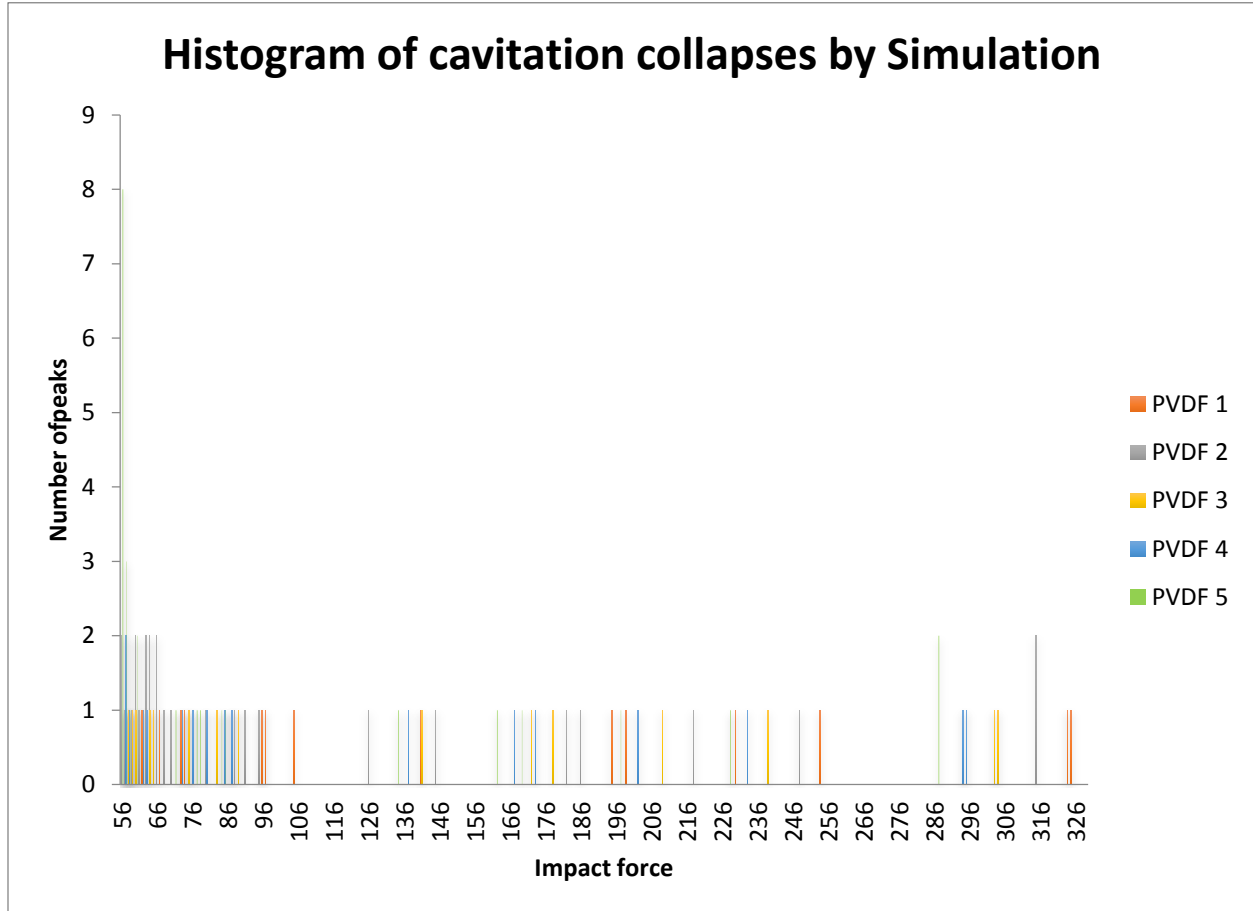


Figure 10.8 Histogram of cavitation collapses by simulation

These results are considered for same regime which used in experiment. But the time period of simulation is 1 second. By analyzing histogram, all PVDF film can detect strong the cavitation bubble cloud collapse because effect of bubbles collapse affects whole region of blade. But the all weak collapses are not detected by 1st PVDF and 2nd PVDF film. It can be shown in figure. It shows that higher effect of Cavitation occurs near to 5th PVDF film as highest peak number of impact load, which can be shown in figure 10.8.

By comparing both histogram by experiment and by simulation, number of peak for weak collapses are around 4 for experiment in 2 second of time period and 8 for simulation in 1 second of time period. Number of peak for strong collapses is measured 1 by both method of experiment and simulation. By simulation, the strong collapses values are from 280 N to 330 N. and by experiment, the strong collapses values are from 130 to 150 N.

10. SUMMARY:

The work is dedicated to simulation of cavitating flow and its comparison with the experimental measurement.

Cavitating flow occurs due to change of flow direction by obstacle and due to that water pressure drops which is less than its vapor pressure. So that Mass transfer occurs from liquid to vapor and water bubble was created. Than bubble try to increase size till it reach its vapor pressure. When its pressure is higher than its vapor pressure, bubble collapse occurs. Due to collapse, the normal shock produces on surface of obstacle. Due to shock wave, high impact force is developed on surface of obstacle. High impact of force can damage surface of material. PVDF film is be used to measure impact force on blade.

Bubble dynamics is presented by Rayleigh-Plesset equation and mass transfer from water to vapor is measured by Zwart, Schnerr and Sauer model and full cavitation Model.

In experiment, flow rate is 295lt/min, inlet pressure 245 kPa , outlet pressure is 100 KPa, dimension of test section is 150mm×150mm×500mm and angle of attack is 8° and these values are implemented in Fluent .

Turbulence flow is generated near to boundary of blade in test section due to shape of blade or due to pressure difference. K- ω turbulence model is better to give effective result near to boundary condition, but SAS SST model is better than k- ω model. It works at k- ω model near to boundary and it works as k- ϵ in normal turbulent flow.

In experiment, the specific bubble radius was measured by spectrometer so zwarts model of mass transfer is better than other models because this model is flexible as it can be modified by changing the value of bubble radius, volume fraction of nuclei and its vapor pressure. The result from simulation has good quality which is quite similar to the experiment. Here, time period of experiment is 2 second and sampling frequency is 100 KHZ but it consumes more time and memory of computer if same data used for simulation. So time period of simulation is 2 second and frequency is 1 kHz are selected for simulation.

The mechanism of cavitation is quite similar by both experiment and by simulation which is compared by the visualization and by the force signal from each PVDF film. From both methods, we observed that the cavitation is increasing from leading edge of blade to the trailing edge of blade. AT constant Reynolds number, cavitation is increasing with increasing cavitation number. At higher cavitation number, cloud cavitation observed and at low cavitation number, no cavitation occurs in flow.

A method of data analysis based on Histogram of impact forces which is used to get to know higher number of peaks at specific impact load. This method describes the strongest impact force which is measured near to leading edge of blade, and fluctuation in impact force by cavitating flow is higher at trailing edge of blade. The comparison of Histogram gives information about difference in number of pick values at specific impact force by Experiment and by simulation. At week collapses number of peak of impact are quite similar but by simulation, due to the strong collapses, impact forces are higher

compare to the result from experiment. It is possible that impact force due to strong collapses are higher because in simulation fluid is considered as incompressible fluid and there is no damping is used. Or calibration of signal of PVDF films was incorrect. Signal can be recalibrated for each PVDF film of experiment by using histogram of PVDF films from Simulation.

This work has one limitation where time period of one cavitation mechanism by simulation is quite higher compare to result of experiment, which is effected by time step value, vapor pressure, nucleation volume fraction and bubble diameter. Simulation of the model can be more improved by modified cavitation model and by reducing time size.

FFT result shows that same amplitude value at same frequency of bubbles collapses for experiment and for simulation. But, PVDF film by experiment cannot able to sense frequency at low frequency bubble which has higher amplitude. It can be modified by recalibrate PVDF film from simulation data of PVDF films.

11: CONCLUSION:

The numerical simulation and experimental model shows similar results for the selected cavitation regime.

It shows good agreement of the result of impact load by experiment and simulation. The work presents that similar mechanism of cavitation developed by experiment and by simulation by method of visualization and by signals. This work also represents that how cavitation is influenced by cavitation number for corresponding Reynolds number.

The histogram of impact force is used to determine the impact loads. By this method, fluctuation in impact force by cavitating flow is higher at trailing edge of blade. By comparing experiment and by simulation, numbers of peak of weak collapse are almost similar but strong collapse impacts is higher by simulation compare to Experiment

By comparing FFT analysis, PVDF films cannot sense collapses at low frequency of bubbles in experiment which shows that PVDF films calibration is not correct. This can be improved by using signal of impact force of simulation.

Simulation model can be modified by reducing time step and by improving mass transfer model in cavitation.

12. ABBREVIATION AND NOMENCLATURE:

Abbreviation:

PVDF = polyvinylidene difluoride

RNG = renormalization group

SST = Shear-stress transport

RSM = Reynolds stress modeling

DES = Detached eddy simulation

LES = Large eddy simulation

SAS = Scale adaptive simulations

RKE = Realizable k- ϵ

CFD = Computation fluid dynamics

RANS= Reynolds averaged Navier-Stokes

Nomenclature:

σ = Cavitation Number

P_0 or P_a = ambient static pressure

P_v = vapor pressure

u = velocity of fluid

ρ = density of fluid

R = Radius of nuclei

T_{ν} = surface tension

R_b = Radius of bubble

ρ_l = liquid density

p_b = bubble pressure

ρ_v = vapor density

U = instantaneous velocity of fluid

P = instantaneous pressure of fluid

τ = stress tensor

S_M = addition sources of momentum

m = mass transfer due to cavitation

r_{nucl} = nucleation site volume fraction

F_e = empirical calibration co-efficient for evaporation process

F_c = empirical calibration co-efficient for condensation process

f_v = vapor mass fraction

k = Turbulence kinetic energy

n_b = number of bubbles

α = vapor volume fraction

ϵ = rate of heat dissipation

ω = specific rate of heat dissipation

A = cross-section area of test-section

Re = Reynolds number

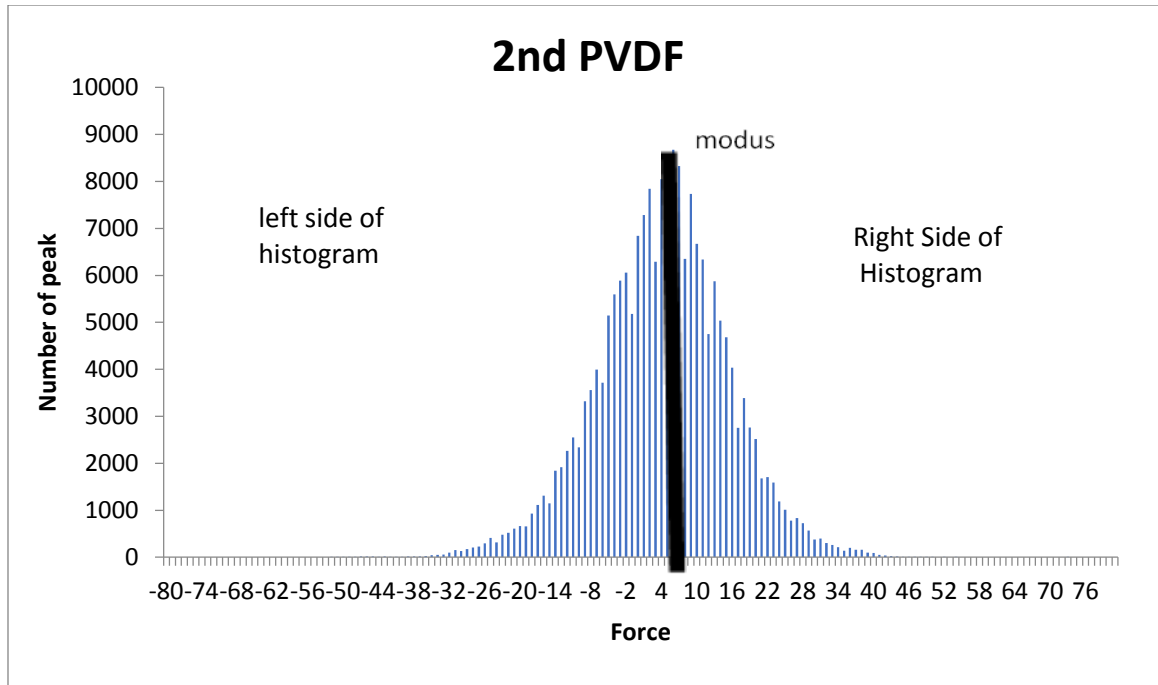
Q = flow rate

13. References:

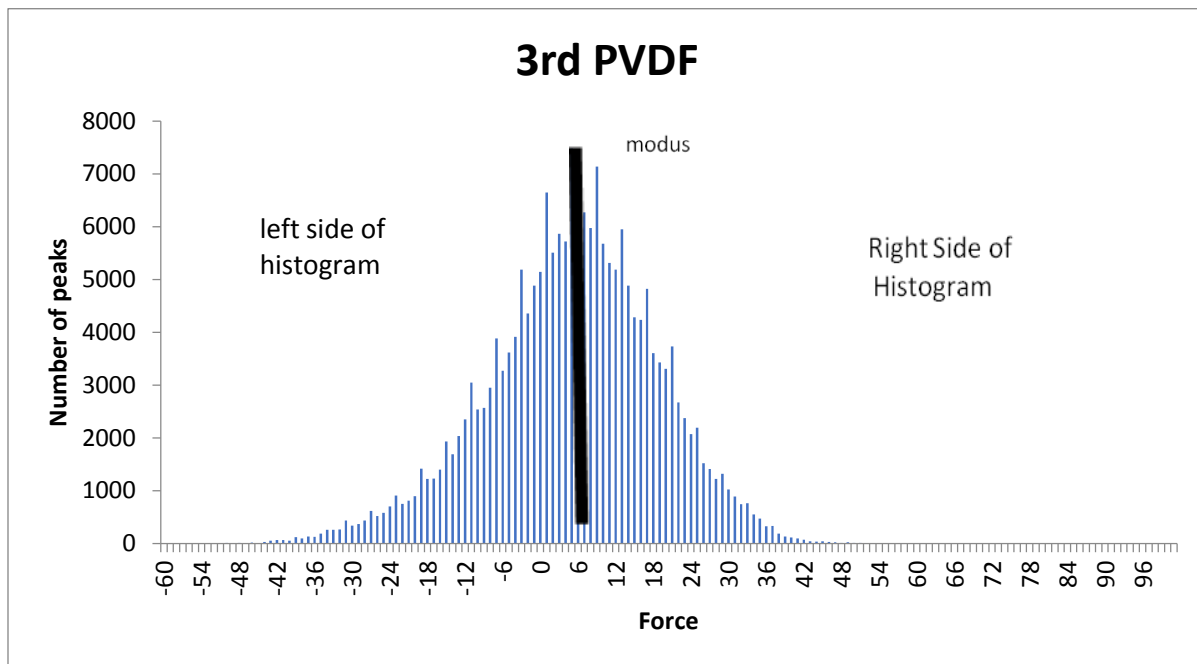
- [1] F. Ronald Young cavitation, imperial collage press, 1999.
- [2] Phillip Eisenberg 'mechanics of cavitation' Mcgrow-Hill book, Section 12 , 1961.
- [3] Christopher Earls Brennen, cavitation noise, 'The internet book of fluid dynamics' 2016.
- [4] Hiroharu Kato, Research paper about Possibility of quantative prediction of cavitation erosion without model test.
- [5] S.T. Chiang and J.H.Chen, Research paper about comparison of different cavitation models on development of 2-D cavitating flow
- [6] Fortes-Patella, Research paper about Approach to Evaluate the Cavitation Erosion Power.
- [7] Tom J.C. Van Terwisga, Cavitation Erosion- A review Model mechanism and erosion risk models.
- [8] ANSYS Fluent Theory Guide book,
- [9] R. Marek and J. Straub, Analysis of the evaporation coefficient and the condensation coefficient of water
- [10] Christopher E. Brennen, Cavitation and Bubble Dynamics, Oxford University press, 1995.
- [11] Jean-Pierre Franc, Fundamental of cavitation, Kluwer academic publisher, 2004.
- [12] Christopher E. Brennen, Fundamental of multiphase flow, Cambridge University press, 2005.
- [13] <http://airfoiltools.com/airfoil/details?airfoil=naca2412-il> .

APPENDIX:

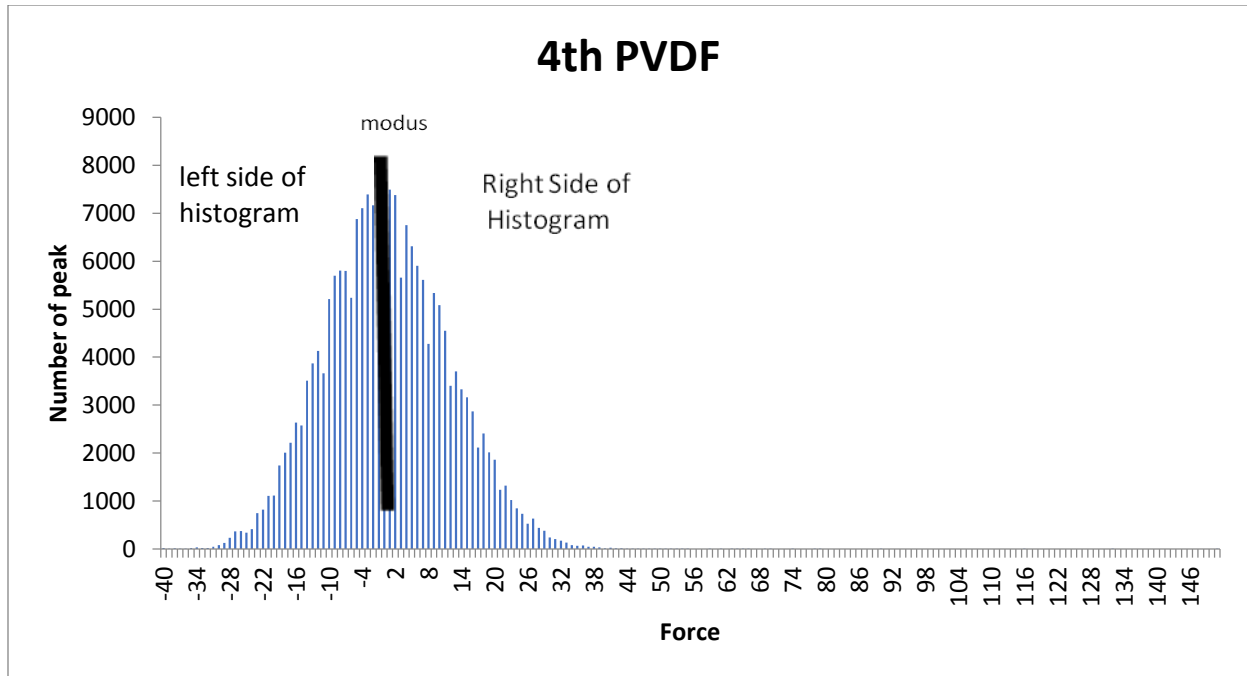
(a) Histograms of Impact force detected by each PVDF films by experiment:



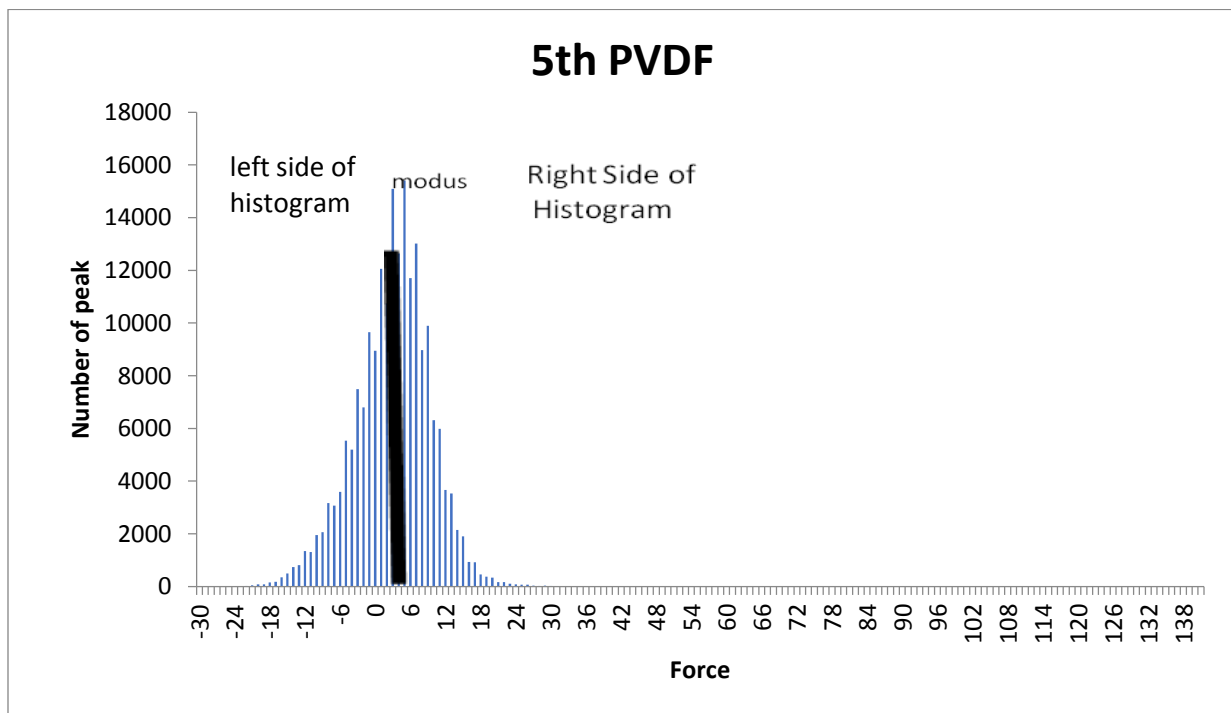
1 Histogram of Impact force detected by 2d PVDF film



2 Histogram of Impact Force detected by 3rd PVDF film

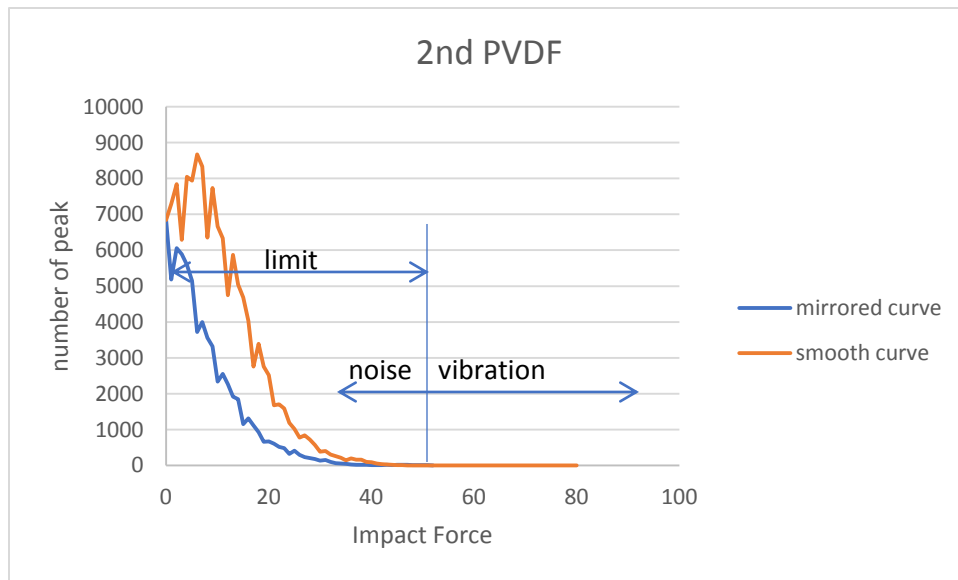


3 Histogram of Impact force detected by 4th PVDF film



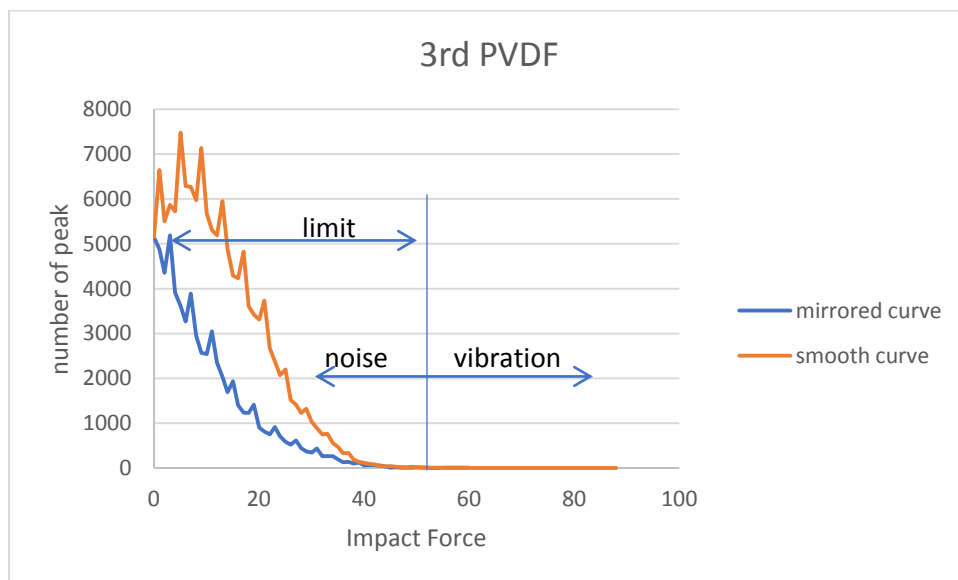
4 Histogram of Impact Force detected by 5th PVDF film

(b) Modified Histogram of impact force for each signal of PVDF film:



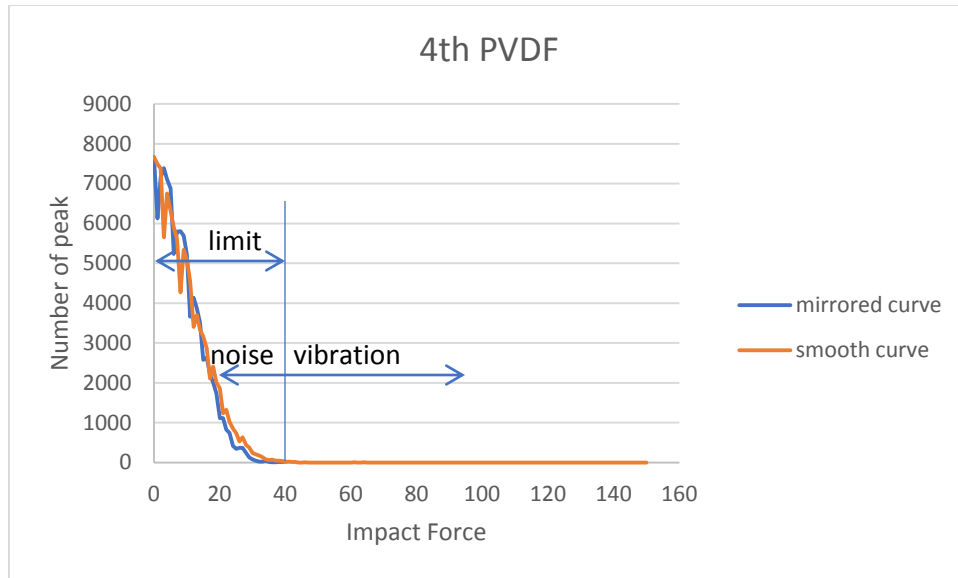
5 Modified Histogram of impact force at 2nd PVDF film

Here as shown in figure 5, the limit impact force at 2nd PVDF film is 52 N.



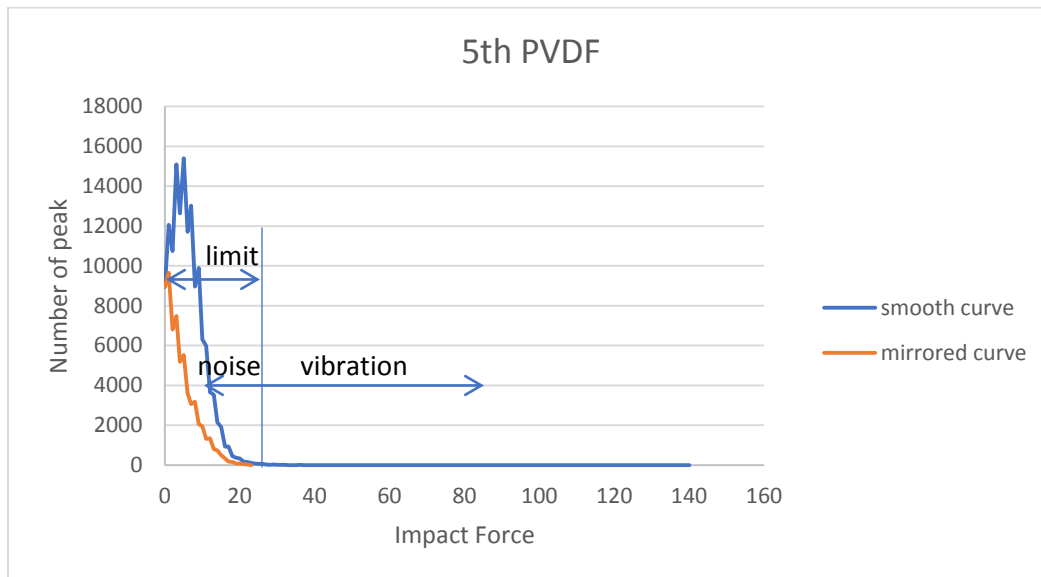
6 Modified Histogram of impact force at 3rd PVDF film

Here as shown in figure 6, the limit impact force at 3rd PVDF film is 55 N.



7 Modified Histogram of impact force at 4th PVDF film

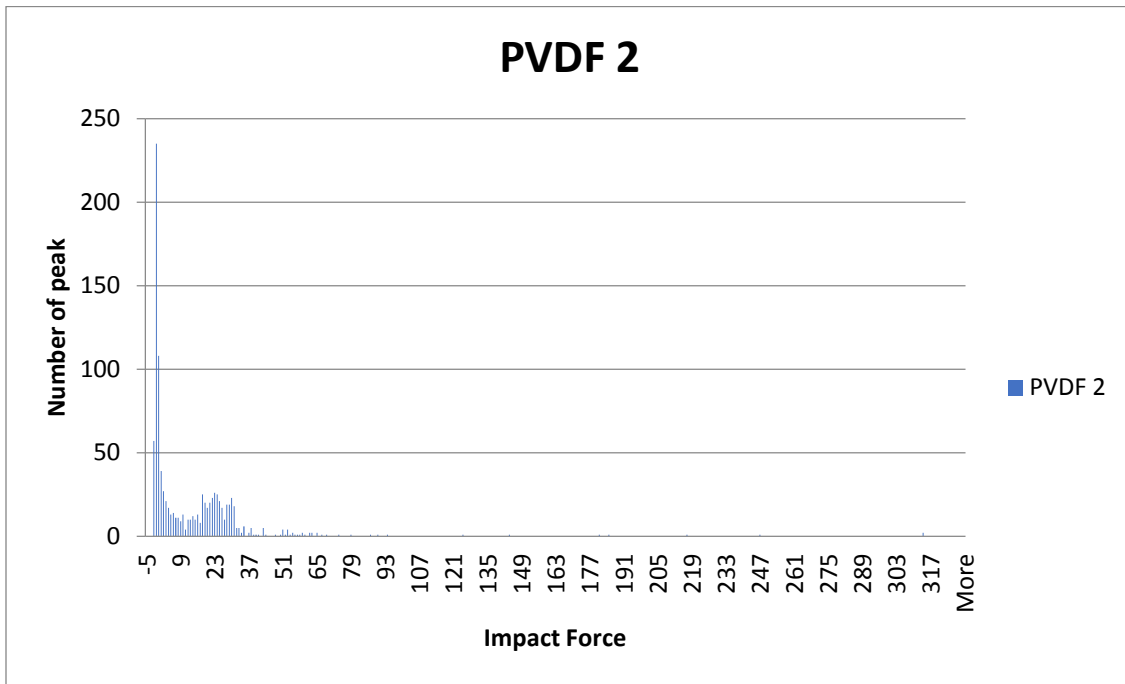
Here as shown in figure 7, the limit impact force at 4th PVDF film is 40 N.



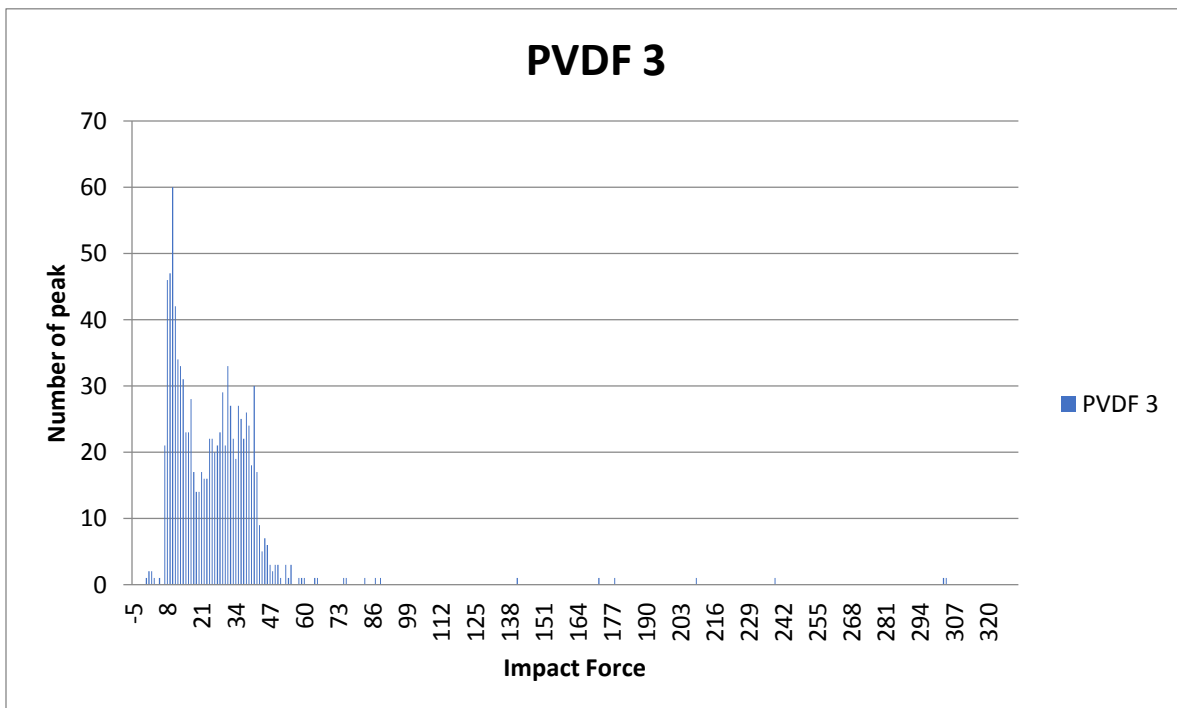
8 Modified Histogram of impact force at 5th PVDF film

Here as shown in figure 8, the limit impact force at 5th PVDF film is 25 N.

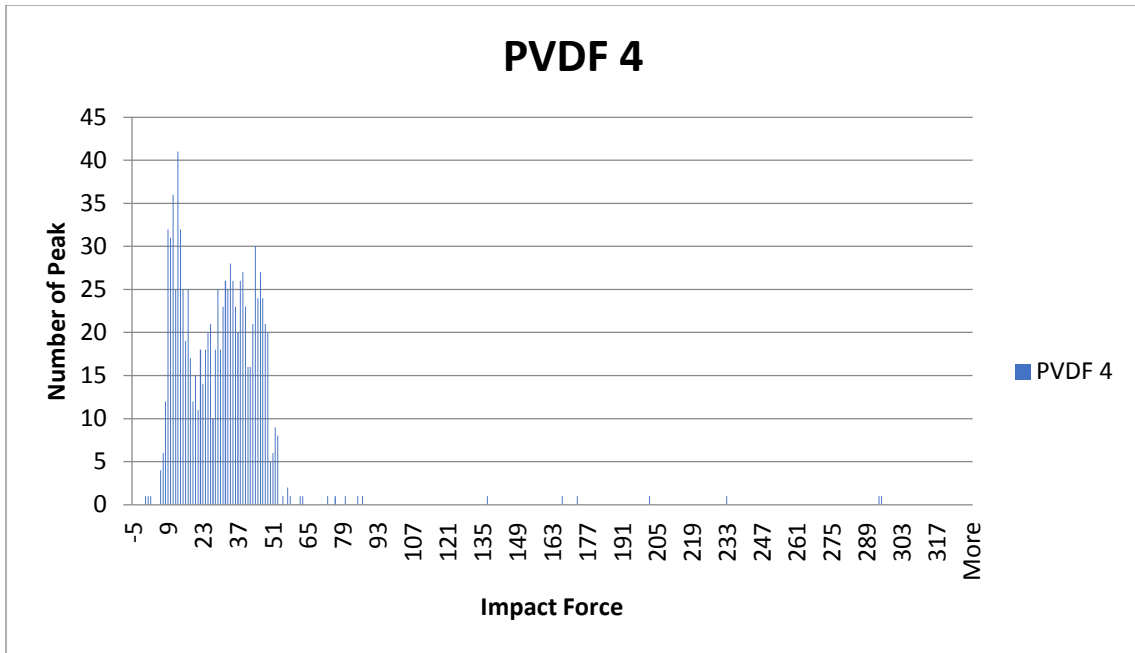
(c) Histogram of impact force signal for each PVDF film by simulation:



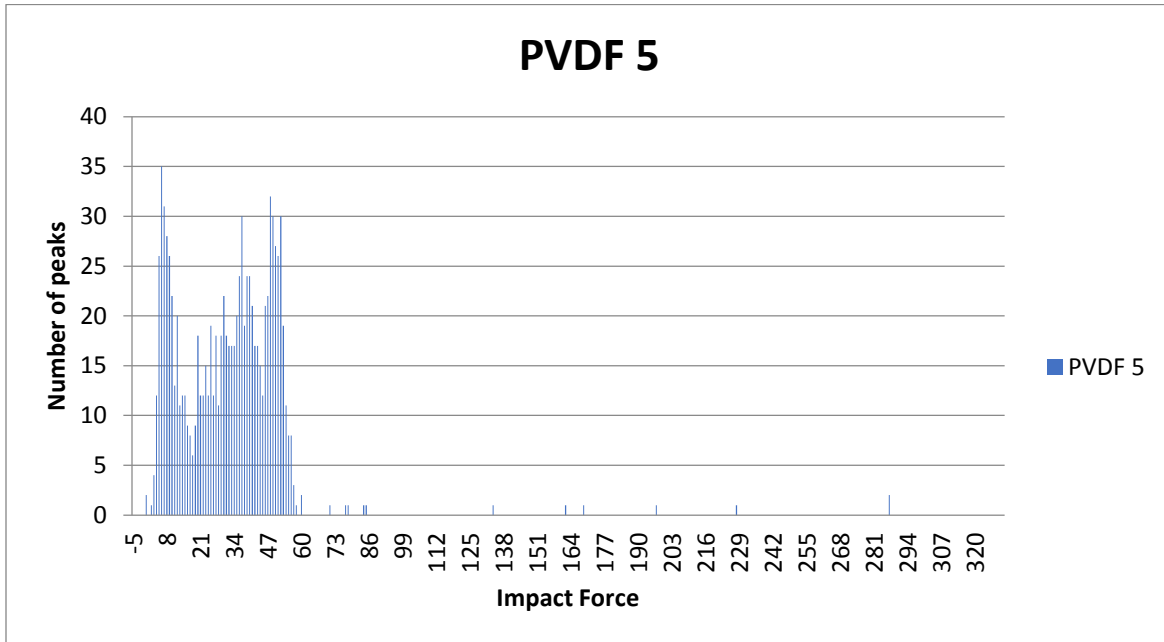
9 Histogram of Impact force detected by 2nd PVDF film



10 Histogram of Impact force detected by 3rd PVDF film



11 Histogram of Impact force detected by 4th PVDF film



12 Histogram of Impact force detected by 5th PVDF film